IMAGE DERIVED INPUT FUNCTION FOR BRAIN [^{11}C]TMSX PET IMAGING

IMRAN ALI WAGGAN

Turun yliopisto
University of Turku

Master's thesis

University of Turku
Faculty of Medicine
Turku PET Centre
Division of Clinical Neurosciences

Master's degree in Biomedical Imaging
Clinical and *in vivo* imaging

Credits: 45 ECTS

Supervisors:

1: Laura Airas, MD, PhD, Professor

2: Eero Rissanen MD, PhD

Examiners:

1: Valtteri Kassinen MD,PhD Adj Prof

2: Eero Rissanen MD, PhD

TURUN YLIOPISTO
Faculty of Medicine, Institute of Biomedicine
Turku PET Centre
Division of Clinical Neurosciences

IMRAN ALI WAGGAN:

IMAGE DERIVED INPUT FUNCTION FOR BRAIN [^{11}C]TMSX PET IMAGING

Master's thesis
Clinical and *in vivo* imaging
APRIL 2019

Modeling and analysis of positron emission tomography (PET) imaging data requires the critical information of the input function of the radioligand used. In PET imaging of the brain, the 'gold standard' for acquiring input function is to estimate the metabolite corrected arterial plasma input of the used radioligand as a function of time via arterial cannulation, i.e. to use the so-called original arterial input function (OAIF) method. Arterial cannulation, however, is unpleasant for the patient, invasive, requires expertise and additional resources. Consequently, it discourages patients and healthy subjects to enroll into clinical PET studies. To counter these problems, the feasibility of an alternative method for acquiring input function from the PET image, image-derived input function (IDIF), was evaluated for brain PET imaging with [^{11}C]TMSX radioligand in this thesis. [^{11}C]TMSX is a radioligand binding selectively to adenosine A_{2A}-receptors. The method was implemented on data from 45 study subjects (9 healthy controls, 19 Parkinson's disease patients and 17 multiple sclerosis patients) imaged with [^{11}C]TMSX and High Resolution Research Tomograph (HRRT) PET scanner in earlier studies in Turku PET Centre. The results showed significant differences between the level of IDIF and OAIF values although with a high correlation. Image derived input function acquisition method that was used in this study is therefore not reliable enough to substitute original arterial input function. Alternative IDIF extraction methods should be investigated for this purpose in the future.

KEYWORDS: Positron emission tomography, input function, [^{11}C]TMSX, Multiple Sclerosis, Parkinson's Disease

To my father, a man with an impeccable character and relentless courage.

ABBREVIATIONS

^{18}F-FDG	*^{18}F-flurodeoxyglucose*
AD	*autosomal-dominant*
AR	*autosomal-recessive*
ARB	*angiotensin-receptor blocker*
AUC	*area under curve*
BBB	*blood-brain barrier*
BDNF	*brain derived neutropenic factor*
BG	*basal ganglia*
cAMP	*cyclic adenosine monophosphate*
CIS	*clinically isolated syndrome*
CM	*compartmental model*
CNS	*central nervous system*
COMT	*catechol O methyl transferase*
CPu	*caudate-putamen*
CSF	*cerebrospinal fluid*
DiCCB	*dihydropyridine calcium channel blocker*
DIS	*disseminated in space*
DIT	*disseminated in time*
DM	*diabetes mellitus*
EAE	*experimental autoimmune encephalitis*
EBV	*Epstein-Barr virus*
EC	*extra-cellular*
ER	*endoplasmic reticulum*
GABA	*γ-aminobutyric acid*
GIT	*gastro-intestinal tract*
GWAS	*genome wide association studies*
HC	*healthy controls*
HRRT	*high resolution research tomograph*
IC	*intra-cellular*
IDIF	*image derived input function*
IgG	*immunoglobin G*
LB	*Lewy bodies*
MAO-B	*monoamine oxidase B*

MPTP	*1-methyl-4-phenyl-1,2,3,6-tetrahydropyridine*
MRI	*magnetic resonance imaging*
MS	*multiple sclerosis*
MTR	*magnetization transfer ratio*
NAWM	*normal-appearing white matter*
OAIF	*original arterial input function*
OPD	*out-patient department*
PBIF	*population based input function*
PDEA	*early stage Parkinson's disease*
PDLN	*late stage Parkinson's disease (non-dyskinetic)*
PET	*positron emission tomography*
PPAR-γ	*peroxisome proliferator-activated receptor gamma*
PTAC	*plasma time activity curve*
RF	*radiofrequency*
ROI	*region of interest*
RRMS	*relapsing remitting multiple sclerosis*
SNARE	*soluble NSF attachment protein receptor*
SNc	*substantia nigra pars* compacta
SPMS	*secondary progressive multiple sclerosis*
SUV	*standard uptake value*
TAC	*time activity curve*

TABLE OF CONTENTS

1 INTRODUCTION

[^{11}C]TMSX([7-*methyl*-^{11}C]-(*E*)-8-(3,4,5-Trimethoxystyryl)1,3,7trimethylxanthine is a radioligand that is highly selective for A_{2A} receptors (A_{2A}R) in the brain. A_{2A}R binding increases significantly during neuronal inflammation and therefore, is an effective marker for diseases such as secondary progressive multiple sclerosis (Rissanen et al., 2013a).

However, before learning further about the role of A_{2A} R's in the pathogenesis of these neuronal diseases, it is important to analyze the radioligand that is being used to study it. There are certain pre-requisites for modeling and analysis of radioligands, the major of them being the input function. The 'gold standard' for acquiring input function is to estimate the metabolite corrected arterial plasma input of the used radioligand as a function of time via blood sampling through arterial cannulation which is distressing for the patients and exposes the researchers to unwarranted radiation (Litton, 1997; Zanotti-Fregonara et al., 2011b). In order to avoid these adverse effects, we investigated an alternative approach for acquiring input function from the dynamic brain [^{11}C]TMSX PET image data co-registered with MRI.

In essence, there are three important steps that are common to all methods of acquiring image derived input function: (1) carotid region of interest (ROI) drawing, which can be done by using co-registered MRI images or segmenting the carotids directly on the PET images. We used the former approach in our study. (2) Partial volume effects correction which is then used for whole blood time activity curve (TAC) calculation. (3) Distinction of parent radiotracer from its metabolites by metabolite correction. This third step requires accurate metabolite analyses and radioactivity measurements as a function of time acquired via blood sampling as the PET scanner cannot distinguish between the original tracer and its radioactive metabolites,

2 LITERATURE REVIEW

2.1 Multiple Sclerosis

Multiple sclerosis is a chronic neuroinflammatory disease which affects, primarily, the long nerve axons resulting in their demyelination that may lead to significant disability. Around 2.5 million people are affected by this disease globally with Northern Europe and Canada having the highest incidence in the world. The disease typically affects young adults and is twice as common in females as compared to males (MS International Federation, 2013).

In majority of the cases, the disease initially presents as relapsing remitting (RRMS) type of disease. The average onset of the disease is in the early thirties. With time, the disease gradually progresses into the secondary progressive disease (SPMS) in most patients within one or two decades. The symptoms of MS are varying depending on the anatomical location of the lesion in the CNS and may include visual impairment due to optic neuritis, sensory and motor symptoms, balance impairment, bladder dysfunction and cognitive deficits such as impairment in executive functioning and long term memory (Compston and Coles, 2008). As the disease progresses, the symptoms progress and accumulate resulting in an increasing disability and impaired quality of life (Menon et al., 2017).

RRMS first manifests as episodes of neurological dysfunction called relapses. In case the diagnostic criteria are not met at the time of the first relapse, the condition is called clinically isolated syndrome. The relapses are followed by a complete or partial remission of the symptoms, hence the term relapsing-remitting (Barnett and Prineas, 2004).

Approximately 10 percent of patients with MS are diagnosed as having primary progressive disease (PPMS) in which the initial symptoms keep on accumulating right from the disease onset. Other less common variants of MS include Balo's concentric sclerosis and Marburg (or tumefactive) MS (Compston and Coles, 2008).

2.1.1 Pathogenesis of MS

The exact cause of MS is still unclear although there is a consensus that it is a combination of genetic factors and yet unidentified environmental triggers that lead to disease onset in susceptible individuals. In genome wide associated studies (GWAS), more or less 100 genetic sites have been identified to be a potential risk factor for developing MS (Beecham et al., 2013).

CNS differs immunologically from the rest of the body as the blood brain barrier (BBB), the tight endothelial barrier between brain vasculature and brain parenchyma and interstitial tissue, restrict the free movement of leukocytes and large molecules from the blood into the CNS.

MS is characterized by the inflammatory lesions, or plaques, located at the site of BBB breakdown due to autoimmune activity. The lesions in the early stages of the disease are thought to result from the presence of autoreactive T-cells, that react with specific autoantigens of the normal brain. These autoantigens include myelin basic protein, myelin oligodendrocyte glycoprotein and others. They are recognized by autoreactive CD 4^+ cells in both normal and the disease population and it is hard to pin point which of these antigens are mainly responsible for the disease.

CD 8^+ T-cells are typically found in larger numbers in the demyelinating lesions as compared to CD 4^+ T-cells. Their overall numbers also closely mimic the actual axonal damage (Frischer et al., 2009). Post-mortem brain samples of patients with SPMS often show significant increase of the tertiary lymphoid structures in the meninges (Howell et al., 2011), which is considered hallmark for chronic inflammation (Drayton et al., 2006). Recent studies have shown increase in leptomeningeal inflammation in PPMS (Choi et al., 2012). Studies have also shown a decrease in the regulatory T-cells in CSF in MS patients (Feger et al., 2007). The cause of this decrease is considered to be the reduction in naive regulatory T-cells in addition to compensatory yet ineffective increase in the population of memory T-cells (Viglietta et al., 2004). The decrease in effector-regulatory cell interaction helps promote autoreactive cells that ultimately leads to CNS damage.

Environmental factors may play a significant role in triggering the emergence of autoreactive T-cells. These factors may include viruses or other microbial organisms that,

according to molecular mimicry hypotheses, will resemble certain myelin-related antigens and may then give rise to the production of auto-reactive T-cells which will attack the myelin within the CNS (Olson et al., 2001; Harkiolaki et al., 2009). According to some *in-vitro* studies, these microbial organisms initiate the production of toll-like receptors which in turn increase the production of IL 12 and IL 23 resulting in the production of auto-reactive T-cells (Waldner et al., 2004). Some environmental factors may indirectly decrease the threshold for auto-reactivity by increasing the pro-inflammatory elements. In some instances, peripheral inflammation can contribute to CNS inflammation via increased production of cytokines. These cytokines are actively transported into the CNS through the BBB and can activate perivascular macrophages and microglia and this will contribute to the initiation of inflammation (Dantzer et al., 2008).

Regardless of the initiating event, inflammation resulting in new white matter lesions is considered as the hallmark of RRMS (Coles et al., 2006). As mentioned before, it results from the introduction of cytokines and chemokines in the brain which is a direct consequence of BBB disruption. Recent study suggests that Adenosine receptor manipulation could potentially help curb the entrance of inflammatory cells to the brain through BBB thus helping in restricting the resultant inflammatory cascade (Bynoe et al., 2015; Carman et al., 2011). Additionally, A_{2A} receptor stimulation may help reduce inflammation by decreasing cytokine production (Vincenzi et al., 2013). The pathology is restricted to the new focal white matter lesions in RRMS and there is little to no disease activity in the cortex or normal appearing white matter (NAWM). Brain atrophy has been noted however during RRMS which may be related to the fatigue experienced by patients during the early stages of the disease (Chard et al., 2002; Marrie et al., 2005).

In SPMS and PMS, in contrast to RRMS, the balance tilts from inflammation towards neurodegeneration. There is a decrease in the number of new lesions, expansion of older lesions, atrophic changes in grey and white matter as well as changes in the NAWM (Frischer et al., 2009; Prineas et al., 2001). It has been concluded that the inflammatory infiltrates that result in the demyelinatory plaques along with grey and white matter changes are derived locally from brain connective tissues and meninges instead of the peripheral tissue because of a lack of observable BBB breakdown in MRI studies (Hochmeister et al., 2006; Choi et al., 2012; Howell et al., 2015). Activated microglia are

strongly linked with demyelination along with neurodegeneration observed in SPMS and PMS (Bø et al., 2003; Airas et al., 2015).

As previously discussed, inflammation, gliosis, axonal loss along with microglial activation results in diffuse injury in NAWM as well as in cortical grey matter (Allen et al., 2001). This may also be associated with ventricular dilatation as a consequence of atrophic changes in the brain. Severity of NAWM injury increases as the disease progresses and has a correlation with the degree of cortical demyelination (Kutzelnigg et al., 2005; Mistry et al., 2014; Haider et al., 2014).

Axonal injury in progressive MS may lead to axonal destruction, chronic demyelination or restorative re-myelination. Axonal destruction results from the loss of neuronal trophic support from other neurons. It may also result from the loss of synaptic input which leads to an increase in the local inflammatory response leading to neuronal degeneration (Banati et al., 2000). Chronic demyelination, in-addition to losing the essential trophic support also cause the migration of Na+ channels from the nodes of Ranvier to the demyelinated segment. This leads to an increase of Na+ which is consequently improperly balanced by Na+ K+ dependent ATPase because of mitochondrial dysfunction. Increased Na+ load results in Na^+ Ca^{2+} antiporter reversal leading to increased Ca^{2+}. This results in an increase of calcium dependent enzymes leading to neurolysis (Franklin et al., 2012; Ransohoff, 2016).

Among the multitude of factors that can increase the risk for developing MS particularly smoking and infectious mononucleosis caused by the Epstein-Barr virus (EBV) are factors that show strong association in promoting MS development (Belbasis et al., 2015). Circadian disruption and vitamin D deficiency may also be among the risk factors for MS (Hedstrom et al., 2011).

Increased level of EBV antibodies and a history of infectious mononucleosis strongly correlates to higher risk of MS (Handel et al., 2010). Studies have postulated several mechanisms for EBV associated MS. It has been suggested that MS may be caused via reactivation of latent EBV infection that leads to activation of effector T-cells (Lossius et al., 2014). In addition to that, chronic viral infection may also result in higher amount of EBV associated memory T-cells which is significantly more noticeable in MS, and especially RRMS (Duszczyszyn et al., 2010). Another possible mechanism is a general

immune system dysregulation by EBV which may ultimately cause MS (Münz et al., 2009).

2.1.2 Signs and Symptoms of MS

MS can present with variable symptoms. According to MS International Federation, 2013 report, patients most commonly present with sensory and motor symptoms. These may include paresthesia, extremity weakness, diplopia, urinary retention or vertigo. Many patients present with painful extra-ocular movements, double vision or loss/reduction in vision usually caused by optic neuritis, another common finding. Some patients may complain about altered sensation in the back when bending the neck anteriorly, also known as the Lhermitte's symptom (Multiple sclerosis in adults: management | 1-recommendations | Guidance and guidelines | NICE).

In the majority of cases the symptoms disappear after a few days or weeks followed by remission as described earlier. Multiple factors may enhance or reduce the severity of symptoms or relapses. Infections are known to exacerbate symptoms while pregnancy is known to reduce or eliminate relapses completely. In stark contrast, the postpartum period may enhance the likelihood of relapses possibly because of the alterations in the function of the immune system taking place after the delivery and due to the increased demands and stresses associated with that period (Papadakis et al., 2017).

2.1.3 Diagnosis of MS

Diagnosis of MS is often difficult and almost never straightforward because of a lack of a single confirmatory test. The signs and symptoms of MS can be caused by multiple diseases and therefore it is imperative that the diagnosis is done carefully and other potential causes are ruled out that may present in the same manner.

To help facilitate the diagnosis of MS, certain pre-requisites have been set which are more formally known as the McDonald Criteria. The 'gold standard' for the diagnosis of MS is magnetic resonance imaging (MRI) with cerebrospinal fluid analysis used as a support to rule out an alternative condition. According to the revised 2017 McDonald criteria, the MRI pre-requisites for diagnosis are subdivided based on the location or timing of the

lesion i.e. according to dissemination in space (DIS) and dissemination in time (DIT) respectively (Thompson et al., 2018).

MRI criteria for DIS states that there should be at least one T2 lesion in 2 to 4 areas of the brain in order to be diagnosed as MS. Areas that are considered as the possible sites for these preliminary lesions include periventricular, spinal cord, juxta cortical and infratemporal areas of the brain.

One of the newer studies confirms earlier research that in a patient with clinically isolated syndrome (CIS) only a single MRI demonstrating DIS, gadolinium enhancing and non-enhancing lesions are enough for determining whether the patient has clinically definite MS (CDMS). It also suggests that in the above-mentioned case MRI showing DIS and gadolinium and non-enhancing lesion can replace the earlier DIT criteria provided that the gadolinium enhanced lesions are not caused by something else than MS. In addition to that, by using the much simplified MAGNIMS criteria, the diagnosis of CIS could be based on just one MRI scan (Montalban et al., 2010). It helps simplify the diagnostic process for the clinician without compromising on accuracy. It is also pertinent to mention that in case the patients don't have gadolinium enhancing and non-enhancing lesions in conjunction, DIT criteria must be applied for diagnosis.

Although not in routine clinical use, it is also now possible to distinguish between active, chronic and slowly expanding lesions by analyzing paramagnetic rims on MRI. Also, longitudinal MTR maybe used to assess the demyelination or remyelination in a patient which contributes significantly to neurodegeneration (Absinta et al., 2016a; b).

CSF examination helps to confirm the inflammatory nature of the white matter focal lesions. CSF findings are considered to be compatible with neuroinflammation if there is an increase in IgG or presence of oligoclonal bands on CSF electrophoresis and mononuclear pleocytosis. A negative CSF finding in terms of neuroinflammation might suggest that the white matter lesions are caused by other etiology, such as ischemia.

2.2 Parkinson's disease

Parkinson's disease is a progressive neurodegenerative disorder. It is believed that it affects almost 1% percent of the population above the age of 65 years (Lang and Lozano, 1998a; b). In Finland, according to case-finding studies, the current prevalence of PD is approximately 300/100,000 (Ylikotila et al., 2015).

2.2.1 Pathogenesis of Parkinson's disease

PD is a multifactorial disease (Figure 1). All the cardinal clinical manifestations of PD occur primarily because of loss of dopaminergic neurons in the brain. The principle area affected is the substantia nigra pars compacta (SNc), a basal ganglia structure located in the midbrain. It is now believed that at the time of first clinical symptoms, there already is a widespread pathology resulting from various different mechanisms before the involvement of SNc, which occurs somewhere in the later stages of PD (Braak et al., 2003). The cardinal pathological feature of Parkinson's is considered to be the presence of Lewy bodies (LBs) in the surviving neurons (Wakabayashi et al., 2007; Shults, 2006). In addition to LBs, Lewy neurites are also found in the surviving structures of the brain. PD has long been considered as an idiopathic disorder of the brain. Recent advances in genetic and epidemiological studies have provided an alternative view to the long held notion that PD is primarily a non-genetic disorder of the brain. Newer studies suggest that Parkinson's, indeed, has a genetic component to its pathophysiological mechanism (Dawson and Dawson, 2003; Shulman et al., 2011; Gasser, 2007; Xiromerisiou et al., 2010).

The cardinal features of PD are tremors, bradykinesia, postural instability and muscular rigidity. Along with these primarily motor symptoms, the disease may also have non-motor symptoms that may include speech difficulties along with neuropsychiatric symptoms (Chaudhuri et al., 2005; Poewe, 2008). These non-motor symptoms along with others are the first to appear in a PD patient, well before the motor symptoms (Berg, 2006; Siderowf and Stern, 2006).

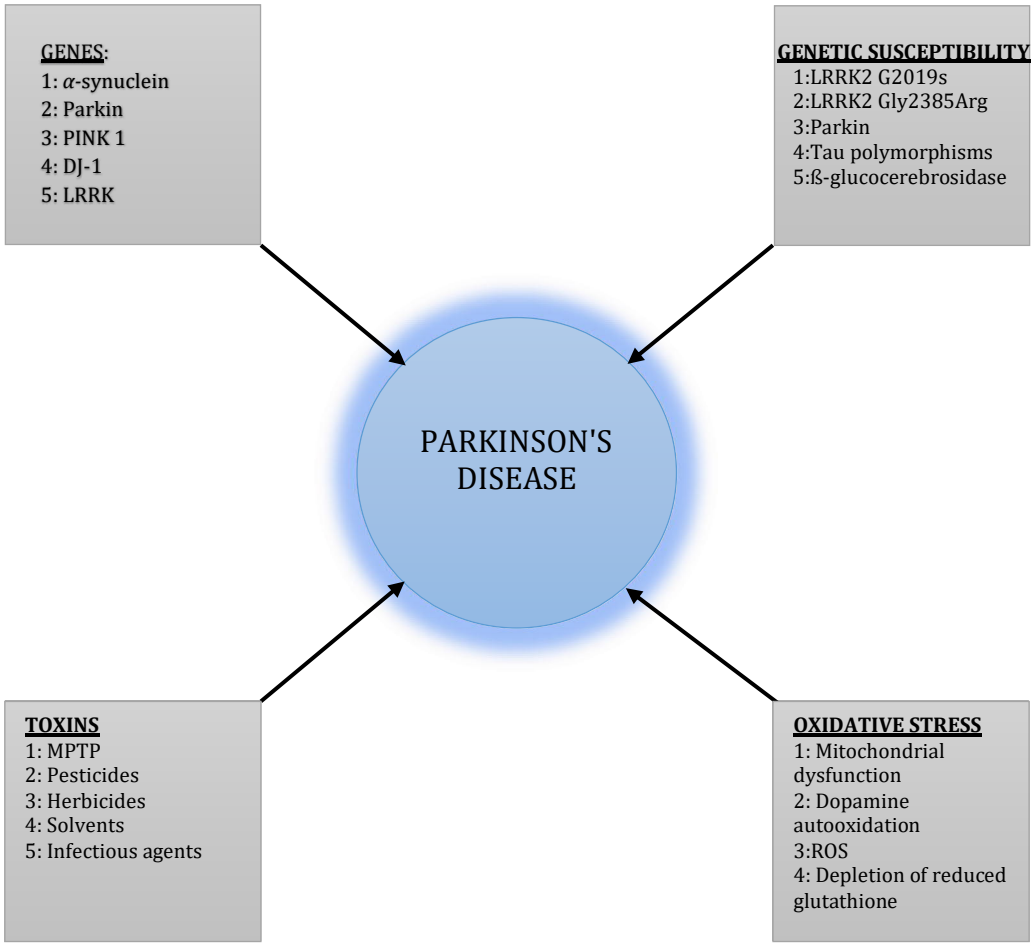

Figure 1 Multifactorial etiology of PD
Modified from (Dalvi et al., 2014)

Motor symptoms of PD arise from the degeneration of nigrostriatal pathway of the brain. Other dopaminergic pathways such as the mesocortical and mesolimbic pathways don't exhibit the same kind of degeneration as nigrostriatal pathways and remain relatively intact. Further, there is widespread cell loss in multiple brain areas. These areas include locus ceruleus, ventral forebrain and raphe nucleus among others. The cell loss leads to an imbalance in noradrenaline, acetylcholine and serotonin in the respective areas (Shulman et al., 2011). Precisely how this culminates into the overall pathology of PD is still not clear.

Although the pathological mechanism of PD is still unclear, there are certain key features that do give us a clue. One of them is the presence of cytoplasmic inclusions also known as Lewy bodies in the neurons (Wakabayashi et al., 2007). The other is microgliosis that indicates neuronal inflammation. This inflammation may contribute to the underlying pathology (McGeer and McGeer, 2008).

Dopaminergic loss in PD can adversely affect a number of processing loops in the brain. These processing loops from cortex to basal ganglia and back to cortex via thalamus are critical in controlling voluntary movements in an organism (Obeso et al., 2004). Dopamine is the major regulatory neurotransmitter in these processing loops as well as other pathways. This signifies the therapeutic advantage of dopamine and the reason for it having the central role in the current symptomatic treatment regimen for Parkinson's disease.

As the disease progresses, however, the treatment regimen becomes more complex primarily because of the chronic use of levodopa (Jankovic and Stacy, 2007). Levodopa starts to show the so-called 'wearing off' and 'on-off' phenomenon. This means that the effect of the drug wears off in a shorter duration of time and the patient has to take higher doses in order to maintain the same effect (wearing off). The on/off phenomenon refers to the unpredictability of the drug itself as the patient oscillates between mobility and immobility. This phenomenon can be alleviated by adding COMT or MAO B inhibitors to the treatment regimen but the effect is not long lasting.

Dopaminergic drugs also have acute and chronic side effects that may include vomiting, nausea to adverse cardiovascular as well as hormonal changes. Dopaminergic drugs may also show adverse neuropsychiatric symptoms such as psychosis and cognitive decline. Recent studies have also shown a large number of patients suffering from compulsive gambling and hyper sexuality. These adverse effects may be attributed to the dysregulation of dopamine (Dodd et al., 2005; Steeves et al., 2009; Stamey and Jankovic, 2008; Pontieri et al., 2015; Weintraub et al., 2010; Voon and Fox, 2007). Dopamine based treatment also tend to increase the incidence of depression and anxiety in a large number of patients (Weintraub et al., 2008).

It is also pertinent to mention here the interaction of A_{2A} receptors and α-synuclein. In a recent study, it was shown that use of selective A_{2A} blockers halts both IC and EC effects and helps reduce α-synuclein induced cellular and neuronal toxicity. In addition to that, A_{2A} receptor inactivation also prevents the adverse effects of α-synuclein on synaptic transmission. This effect may be attributed to the regeneration of glutamatergic NMDA signaling due to A_{2A} receptor blockade. Furthermore, A_{2A} antagonism markedly decreases α-synuclein aggregation (Ferreira et al., 2015). This effect might explain the

neuroprotective effects of Adenosine A_{2A} antagonists which are discussed in detail later in this thesis.

As shown in Figure 1, *parkin* gene is the most common genetic mutation that leads to autosomal-recessive PD. The mutation of this gene is also responsible for initiating PD in adolescents (<20 years) which is termed as juvenile PD. Patients affected with this mutation usually suffer from a relatively earlier onset of disease with a good response to dopaminergic treatment (Gosal et al., 2006). Physiologically, *parkin* is involved in cell's proteolytic pathways. Its mutation may lead to loss of mitochondrial function causing PD (Spratt et al., 2013; Kitada et al., 1998). Parkinson's disease also has an infectious component to its etiology with anti-EBV antibodies showing cross reactivity with α-synuclein in PD patients hypothetically thorough the process of 'molecular mimicry' (Woulfe et al., 2014). Studies show evidence of chronic inflammation in PD affected areas of the brain with reactive microglia despite lack of viral infection (McGeer and McGeer, 2004).

Inflammation is also being studied as one of the cause of neurodegenerative diseases including PD. Microglia are one of the primary mediatory cells for inflammation in CNS. Their activation in SNc in particular is a strong indicator for neurotoxicity (McGeer and McGeer, 2008). Microglia play several roles for mediating inflammation which includes secretion of prostaglandins to a number of different growth factors. They also secrete interferons, interleukins and ROS. These substances may either play a part in neuroprotection or end up enhancing oxidative stress and activating apoptotic pathways. The resulting chronic inflammation make the SNc neurons susceptible to cell death (Schwab and McGeer, 2008). A number of different medications have been hypothesized to protect the brain against this chronic inflammation. These medications include Telmisartan, an ARB, and Thiazolidinediones, an oral anti Type 2 DM drug, which mediates their neuroprotective effect via activation of PPAR-γ (Kurihara et al., 2006; Saavedra, 2012; Ridder and Schwaninger, 2012). In addition to that, Pioglitazones, Rotenone and Isradipine (DiCCB) have also shown promising results in different animal models (Ulusoy et al., 2011).

One more aspect of the pathogenesis of PD is oxidative stress. It's caused by the free radicals produced because of oxidation of dopamine via enzymes as well as external toxins e.g. MPTP. This oxidative stress eventually results in PD and is one of the key

mechanisms that result in the causation of the disease. Oxidative stress can be traced back to neuronal as well as glial sources. Increased production of mitochondrial free radicals is considered the major contributor to oxidative stress. MPTP's inhibition of ETC complex I and genetic mutation like parkin, PINK1 and DJ-1 leads to disruption in mitochondrial function. This suggests that both environmental and genetic factors of PD have a common target i.e. mitochondria for causing the disease.

In conclusion, the pathogenesis of PD is extremely complex involving a lot of different factors using a lot of different mechanisms to inflict damage in a lot of different ways. No wonder it has been termed 'enigmatic' (Woulfe et al., 2014).

2.2.2 Signs and Symptoms of PD

There are four main cardinal symptoms of Parkinson's disease including tremor, rigidity, akinesia and postural instability. Although these are the principle symptoms that are present in a PD patient, there are other motor and non-motor symptoms (Table 1) that may or may not be present alongside these symptoms.

Motor symptoms	*Non-motor symptoms*
Tremor, bradykinesia, rigidity, postural instability	Cognitive impairment, bradyphrenia, tip-of-the-toungue
Hypomimia, dysarthria, dysphagia	Depression, apathy, anhedonia, fatigue, other behavioral and psychiatric problems
Decreased arm swing, shuffling gait, festination	Sensory symptoms: anosmia, ageusia, paresthesias
difficulty arising from chair, turning in bed	Dysautonomia, weight loss
Micrographia, cutting food feeding	Sleep disorders (REM behavior disorder, vivid dreams, daytime drowsiness, sleep fragmentation, RLS)
Glabellar tap reflex, blephrospasm, dystonia, scoliosis, camptocormia	

Table 1 Parkinson's disease symptoms
Modified from (Jankovic, 2007)

2.2.3 Diagnosis of PD

UK PD SOCIETY BRAIN BANK'S CLINICAL CRITERIA FOR PD DIAGNOSIS
Step 1
Bradykinesia
At least one of the following
Rigidity
4-6 Hz rest tremor
Postural instability not caused by either cerebellar, vestibulocochlear, optic or proprioceptive dysfunction
Step 2
Exclude other possible causes
Step 3
Atleast 3 of the following criteria
Tremor at rest, Unilateral onset, Progressive, Response to L-Dopa, Chorea caused by L-Dopa, L-Dopa response for five years +, Over all disease course of 10 years +, Persistent asymmetry mainly on the side of onset

Table 2 Diagnostic criteria for PD
Modified from (Jankovic, 2007)

2.3 Adenosine A_{2A} receptors

Adenosine is a cyto-protective modulator that usually protects the organs or tissues against stress (Haskó et al., 2008). There are multiple ways by which adenosine protects the tissues e.g. vasodilation and resultantly increasing blood supply (Ryzhov et al., 2008), ischemic preconditioning (Cohen and Downey, 2008) and decreasing inflammation by reducing the activation as well as the infiltration of inflammatory cells (Chen et al., 2006). It can also reduce inflammation by decreasing both the production of cytokines as well as free radicals (Martin et al., 2006). Adenosine has four different receptor subtypes: A_1, A_{2A}, A_{2B} and A_3. In human brain, A_1, A_{2A} are the most prevalent receptor subtypes.

2.3.1 Structure of A_{2A} receptors

82.9% base pair homology exists between the A_{2A} receptors of humans and mice. The A_{2A} encoding gene is found on chromosome number 22 in humans (Deckert et al., 1997). In the 2nd intracellular loop of the A_{2A} receptor relative to transmembrane segments 3 and 4 lie two exons and a long intron roughly 6-7.2 kb in length (Peterfreund et al., 1996). In

all the tissues where A_{2A} receptors are located they exhibit one hybridizing transcript (Stehle et al., 1992). It is also pertinent to mention that not only are A_{2A} receptors polymorphic but also contain a silent mutation in certain populations. This T1083C mutation is found to be more common in Caucasians as compared to Asians (Le et al., 1996; Deckert et al., 1996).

2.3.2 A_{2A} receptor distribution

It is important to understand the distribution of a particular receptor in order to understand where the agonists as well as antagonists would act if they were given to an organism. Higher number of receptors almost always correlates with greater efficacy of agonists (Kenakin, 1995). To put it in context of adenosine, because of its low quantity, it may be able to trigger a response where A_{2A} receptors are abundant but won't be able to do the same where receptors are low.

In a normal human brain A_{2A} receptors are primarily located in deep grey matter. They have the highest density in basal ganglia mainly in putamen. This number is closely followed by caudate nucleus and thalamus. Cerebral cortex especially frontal lobe has the least density of A_{2A} receptors in a healthy human brain (Ishiwata et al., 2005; Naganawa et al., 2007; Sakata et al., 2017b).

In patients with MS the density of A_{2A} receptors increases in the NAWM (Rissanen et al., 2013b). Similarly, in Parkinson's disease the density of A_{2A} receptors increases in caudate and putamen specifically in patients experiencing levodopa induced dyskinesia. No increase in receptor density was observed in PD patients under dopaminergic treatment without dyskinesia compared to healthy controls (Ramlackhansingh et al., 2011). Also there is an increase of adenosine A_{2A} receptors on the lymphocytic membranes in PD (Casetta et al., 2014). A similar increase is also seen in patients suffering from MS (Vincenzi et al., 2013).

Adenosine A_{2A} receptors are also found in cardiac tissues as well as alveoli of lungs. Activation of A_{2A} receptors in both organs helps suppress inflammatory cascade thus preserving vital function (Toufektsian, 2005; Alfaro et al., 2017). Adenosine A_{2A} receptors are also present in abundance in brown adipose tissue as well as in skeletal

muscles in comparison to other adenosine receptors (Gnad et al., 2014; Lynge and Hellsten, 2000).

The receptors are also present and functionally important in the GABAergic areas of the hippocampus, dorsal striatum and cortex (Rosin et al., 1998). Receptor density of A_{2A} receptors is significantly higher in the cortex as well as hippocampus in comparison to other adenosine receptors e.g. A_{1A}. In addition to dopaminergic and GABAergic, some studies confirm presence of A_{2A} receptors in cholinergic neurons as well using in situ hybridization (Dixon et al., 1996) and PCR (Richardson et al., 2000). Other studies, however, suggest that there is a lack of A_{2A} receptors in both cholinergic and/or GABAergic interneurons (Augood and Emson, 1994). There is no clear explanation for these contradictive findings.

Multiple methods have been used over the years to unveil the distribution of A_{2A} receptors in the body. Use of radioligands is one of the most effective of these methods. Other methods include using antibodies to locate A_{2A} receptors in striatum, immunohistochemistry in carotid bodies, T-cells (Koshiba et al., 1999) for cardiovascular tissues (Marala and Mustafa, 1998; Gauda et al., 2000), angioblasts of dog's retina (Taomoto et al., 2000), human GIT (Christofi et al., 2001) and nerve terminals of hippocampus in rodents (Rosin et al., 1998). Adenosine A_{2A} receptors are closely associated to plasma membrane as well as cytoplasmic structures which shows that the receptor is actively trafficked within the cell. A_{2A} receptor trafficking in the striatum is still not clear and needs to be studied.

Age also plays a significant role as far as receptor density is concerned in different areas of the brain. Studies performed on the striatum of aged rats show a decrease in the over-all numbers of A_{2A} receptors (Cunha et al., 1995). Age may also effect the glutamatergic, dopaminergic and GABAergic nerve terminals and the activity of A_{2A} receptors within them (Corsi et al., 1999). If we look at these findings together, we can infer that there maybe an imbalance between the A_{2A} (excitatory) and A_1 (inhibitory) receptor mediated effects with age. In stark contrast to striatum, there is an increase of A_{2A} receptors in the hippocampus and a concomitant decrease in BDNF associated tropomyosin-related kinase receptors. This results in an increase in the hippocampal BDNF mediated synaptic transmission (Diogenes et al., 2007). Recent PET study, however, partially contradicts these findings and suggests that although there is a decrease in A_1 receptors, they found

no significant difference in the receptor density of A_{2A} in between younger and older subjects (Mishina et al., 2012).

2.3.3 A_{2A} receptor signaling

Adenosine A_{2A} receptors are G-protein coupled receptors. They have usually been considered to be coupled with the stimulatory type of G-proteins. Other studies show, however, that they may be coupled to different type of G-proteins based on their location in the body (Kull et al., 2000). It is predominantly coupled to the stimulatory type of G-protein in the peripheral tissues. The number of stimulatory type of G-protein is low in the A_{2A} receptor rich areas of the brain such as the striatum. Here the A_{2A} receptors are mostly coupled with G_{olf}, a different class of G-protein. Activation of G-protein coupled proteins by A_{2A} receptors result in the production of cyclic AMP. It may also result in the mobilization of intracellular Ca^{2+}. Inhibition of chemotaxis occurs via A_{2A} receptor activation on neutrophils (Sullivan et al., 2001). Activation of adenosine A_{2A} also result in a mitogenic effect in vascular endothelial cells. This effect is largely mediated by A_{2A} activation of ERK1/2 (Sexl et al., 1997). Stimulatory G protein coupled adenosine A_{2A} receptors are known to desensitize quickly. This effect is believed to be mediated by multiple mechanisms such as Thr 298 phosphorylation via receptor kinases. In addition, phosphorylation by cyclic AMP dependent kinase is also considered to be involved in the rapid desensitization of adenosine A_{2A} receptor (Palmer and Stiles, 1997).

2.3.4 A_{2A} receptors in Parkinson's disease

As previously described, Parkinson's disease is one of the most common age related neurodegenerative diseases. Dopaminergic drugs are the main stay treatment for Parkinson's disease along with MAO inhibitors and COMT inhibitors.

Although dopaminergic drugs are effective in providing symptomatic relief and are still widely used as the primary treatment in PD, they fail to stop its progression. New treatments are needed to stop or at least slow down the progression of this debilitating disease. Because of the excessive expression of A_{2A} receptors in the basal ganglia, the primary site of pathology in Parkinson's disease, A_{2A} antagonists were considered as an alternate to dopaminergic drugs for the treatment of Parkinson's (Pinna, 2014).

Caudate-putamen (CPu) has the highest expression of A_{2A} receptors as compared to other parts of BG. Normally CPu excites striatopallidal neurons which is inhibited by dopamine. In PD, with lack of dopamine, there is an imbalance in these neuronal pathways with striatopallidal neurons getting hyper-excited because of a lack of inhibition from dopamine. These striatopallidal neurons have an inhibitory effect on globus pallidus which normally has a stimulatory effect on thalamus.

Furthermore, there is decrease in the activity of striatonigral pathway, because of lack of dopaminergic stimulation, which also normally excites thalamus. This decrease in the excitatory impulses to thalamus by both globus pallidus as well as striatonigral pathway because of their own inhibition due to lack of dopamine, leads to hypokinetic movements, a characteristic symptom of PD. This pathway is illustrated in Figure 2.

This pathway helps clarify how A_{2A} receptor antagonists work. Antagonism of these receptors leads to a decrease in their excitatory effect on striatopallidal neurons which in turn leads to a decrease of its inhibitory effect on globus pallidus. Excitation of thalamus and a decrease in hypokinetic movement ensues. A_{2A} receptor antagonists bring back some form of balance to these pathways which is disrupted because of lack of dopamine (Jenner et al., 2009; Mori, 2014).

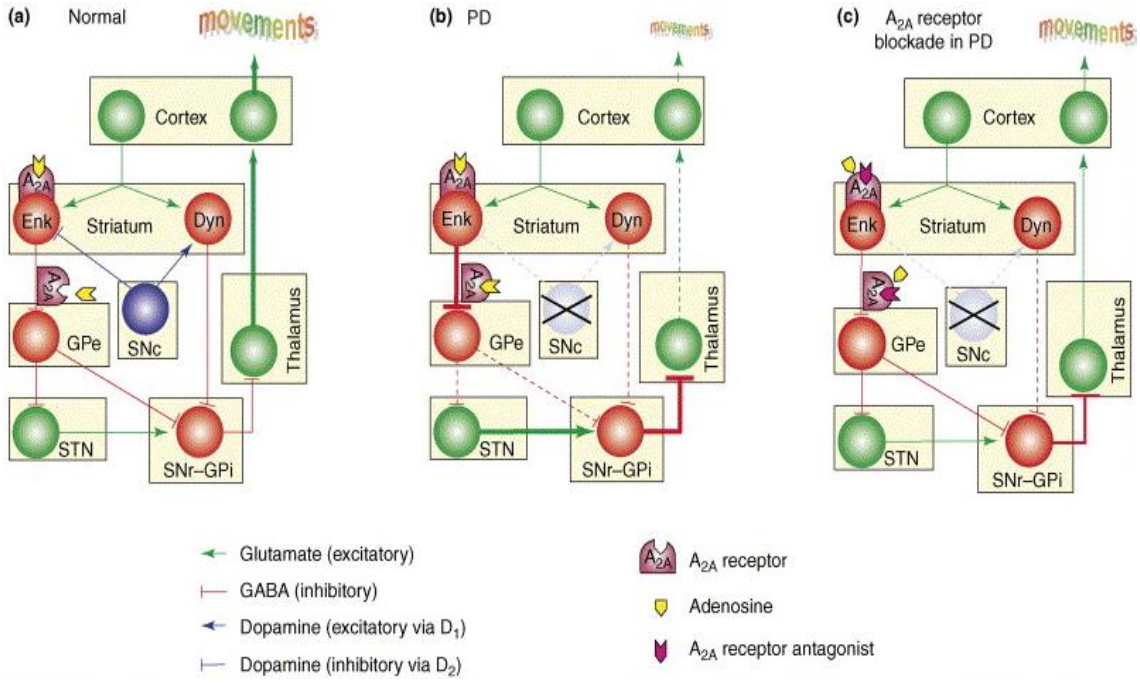

Figure 2 Mechanism of A_{2A} receptors in PD
Reprinted from Trends in Neurosciences, Vol 29, Michael A. Schwarzschild,Luigi Agnati,Kjell Fuxe,Jiang-Fan Chen,Micaela Morelli, Targeting adenosine A2A receptors in Parkinson's disease, Page No. 8., Copyright (2006), with permission from Elsevier

Synergistic action of A_{2A} receptor antagonists and metabotropic glutamate subtype 5 (mGlu5) antagonists has also been reported to improve motor symptoms in PD (Kachroo et al., 2005; Coccurello et al., 2004). A_{2A}-mGlu5 heteromers have also been recently identified in caudate-putamen. This further solidifies the importance of A_{2A}-mGlu5 antagonists in the treatment of Parkinson's disease in future.

There are several xanthine and non-xanthine derivatives that are currently under clinical trials (Table 3) for use in treatment for Parkinson's. There are several other drugs apart from the ones already mentioned in Table 3 that are in different stages of development.

Istradefylline (NOURIAST®), a xanthine derivative, is the only drug among the multitude of drugs mentioned in Table 3 that has been approved for manufacturing and clinical use, mainly in Japan. It has proven to improve the *'wearing off'* phenomena when given as an adjunctive therapy alongside L-DOPA containing drugs in various clinical drug trials . The drug is manufactured as 20 mg tablets and must be taken as a single tablet daily alongside L-DOPA. If symptoms persist, however, the daily dosage could be doubled (Kyowa Hakko Kirin Co., 2013). In various clinical studies, Istradefylline was shown to have relatively good tolerability and safety profile. The most common adverse effects noted with Istradefylline therapy were nausea, dizziness and insomnia along with a possible worsening of dyskinesia. Some patients in the clinical trials also complained of other adverse effects such as headaches and hallucinations. No differences in baseline cardiac and blood chemistry values were noticed among treatment and control groups (LeWitt et al., 2008; Mizuno and Kondo, 2013; Pourcher et al., 2012; Kondo and Mizuno, 2012; Kyowa Hakko Kirin Co., 2013). In one of the clinical trials it was found that the incidence of somnolence, a common adverse effect in patients undergoing treatment for PD with dopaminergic drugs, lowered when patients were treated with high dose of Istradefylline as compared to controls and low dose treatment (Pourcher et al., 2012). This finding is consistent with previous studies which describe the role of A_{2A} based drugs on sleep (Ferré et al., 2007).

Studies have consistently shown the positive benefits of using A_{2A} antagonists alongside L-DOPA based treatments for PD. They have been consistent in reducing *'off-time'* by almost one hour per day in patients with advanced Parkinson's disease. The current treatments e.g. MAO-B inhibitor, rasagiline and COMT inhibitor entacapone, however,

show similar kind of results when used adjunctively with levodopa. It should also be noted that in all of the clinical trials A_{2A} antagonists were used alongside drugs such as MAO-B inhibitors and COMT inhibitors so it is hard to attribute the benefits to the use of A_{2A} antagonists alone. The effects of A_{2A} antagonists without co-treatment of non-dopaminergic PD treatments must be studied in order to correctly determine the positive effects of these drugs. One more factor that needs to be closely examined is the consumption of coffee and other caffeinated beverages in the study subjects, since caffeine is a non-selective adenosine receptor antagonist. At normal consumption levels, coffee interacts with striatal A_{2A} receptors to the same extent as drugs specific to A_{2A} receptors. Therefore, it can be concluded that caffeine consumption might interfere with co-administered A_{2A} antagonists.

Drug	*Company*	*Phase*
ISTRADEFYLLINE	*Kyowa Hakko Kirin Co. Ltd*	*Approved (JAPAN)*
PBF-509	*Palo-Biofarma S.L.*	*Phase I*
ST1535, ST4206	*Sigma-Tau*	*Phase I*
TOZADENANT	*Accorda Pharmaceuticals*	*Phase III (HALTED)*
V81444 (Now CPI-444)	*Vernalis PLC*	*Phase II*

Table 3 *Names, associated companies and development phase of A_{2A} receptor drugs in clinical trials. Table modified from (Pinna, 2014)*

As previously mentioned, the current treatment regimen for Parkinson's disease does little to stop the neuronal degeneration, specifically of the dopaminergic neurons, which is the pathological basis of PD. Recent studies emphasize that blocking A_{2A} receptors may help stop this neuronal degeneration (Chen et al., 2007). Although the neuroprotective effects of A_{2A} antagonists have been observed in animal models, the exact mechanism with which these effects manifest in humans is yet to be ascertained and needs further investigation. In addition to lack of neuroprotective effects, the current treatment also has no effect on cognitive decline. This includes memory deficits experienced by patients relatively early in the disease as well as overt dementia in the later stage. L-DOPA has little to no effect on cognitive decline in PD. A_{2A} antagonists, however, have shown promising results in countering cognitive decline in animal models. A_{2A} antagonists work to improve cognitive function either by deleting the A_{2A} receptor gene or by inhibiting their signaling (Gimenez-Llort et al., 2007). Some studies also suggest that A_{2A}

antagonists may have a positive effect on reward centers of the brain in addition to areas of executive function (Takahashi et al., 2008).

2.3.5 A_{2A} receptors in Multiple Sclerosis

As previously described, multiple sclerosis is a chronic inflammatory disease which primarily effects the central nervous system. It is characterized by scattered plagues of demyelination alongside neuronal damage and gliosis (Dutta and Trapp, 2007). Increased levels of adenosine in cerebrospinal fluid has been found in patients with multiple sclerosis (Tumani et al., 2009; Lazzarino et al., 2010). A_{2A} receptors are found in immune as well as neuronal cells in the central nervous system. However, it still remains to be confirmed whether the activation or blockade of A_{2A} receptors would lead to protection against MS. In EAE, a model to study multiple sclerosis in animals, administration of A_{2A} antagonist leads to a relatively milder course for experimental autoimmune encephalitis. Genetic deletion of CD73, which is known to produce adenosine, yielded similar results (Mills et al., 2008). Subsequent studies, however, showed that loss of A_{2A} receptors, lead to an exacerbation of the disease (Yao et al., 2012).

Increased expression of A_{2A} has also been noted in the peripheral lymphocytes in patients with multiple sclerosis. Stimulation of these receptors may lead to a marked reduction of pro-inflammatory substances such as TNF-α, IFN-γ and others (Airas et al., 2007; Vincenzi et al., 2013).

Recent study shows that the role played by A_{2A} receptor depends on the stage of the disease. In early stages, it protects against MS by providing an anti-inflammatory response specifically on T-cells. In stark contrast to its role in the earlier stage, A_{2A} receptor activation may lead to tissue damage within the confines of the inflamed central nervous system in the later stage of the disease, according to a study conducted on the EAE model (Ingwersen et al., 2016). This finding must be taken into account while developing novel MS treatments based on A_{2A} receptors as has been suggested in previous studies (Du and Xie, 2012). Apart from using A_{2A} receptors as target for new therapies in multiple sclerosis and Parkinson's disease, it can also be used to study pathological mechanisms *in vivo*.

2.3.6 Radiotracers for A_{2A} receptors

[^{11}C]TMSX [7-*methyl*-^{11}C]-(*E*)-8-(3,4,5-Trimethoxystyryl)-1,3,7-trimethylxanthine is one of the most commonly used radiotracer used to visualize A_{2A} receptors to date. Apart from [^{11}C]TMSX, there are multiple other radiotracers used to target A_{2A} receptors, important of them will be described here. A_{2A} receptor radiotracers could mainly be categorized into xanthine and non-xanthine derivatives. Amongst the earliest xanthine derivatives are 3,7-dimethyl-1-propylxanthine (DMPX) and (E)-8-(3,4-dimethoxystyryl)-1,3-dipropyl-7-methylxanthine (KF17837) which were used for neurophysiological and pharmacological studies for A_{2A} receptors. The important non-xanthine derivative is [^{11}C]SCH442416 which was made via O-[^{11}C]methylation using SCH442416 with its 4-mthoxyphenylpropyl group.

[^{11}C]TMSX has been found to be more stable than [^{11}C]SCH442416 and [^{11}C]KW6002 in human plasma. Dynamic PET scans carried out on monkeys showed that striatal uptake was 10 times higher and clearance was faster when compared with [^{11}C]KF17837. [^{11}C]SCH442416 showed better CNS kinetics which is useful for better quantification and evaluation of ligand-receptor binding. [^{11}C]TMSX, however, was found to represent CNS kinetics better when compared with [^{11}C]KF21213. In addition to the PD studies reviewed earlier, other human in *vivo* studies using [^{11}C]TMSX, it has been found that there was an increase in the receptor density in heart and skeletal muscles in males who were endurance trained compared with controls. In another recent study with [^{11}C]TMSX it was noted that the correlation between EDSS scale and MS lesion load with A_{2A} receptor binding in NAWM in SPMS patients was better when compared to the 'gold standard' magnetic resonance imaging parameters (Rissanen et al., 2013b).

Recently, fluorinated analogs of SCH442416 and [^{11}C]preladenant were evaluated as PET ligands in rat brains with both of them demonstrating fast tracer kinetics but the latter showing better A_{2A} quantification (Khanapur et al., 2017; Zhou et al., 2017). In another study, [^{11}C]preladenant was also shown to be safe in human subjects (Sakata et al., 2017a). ^{18}F-MNI-444 has shown the most promising results compared with all the radiotracers that have undergone human trials with high BP_{ND} values in areas rich with A_{2A} receptors along with exceptionally good brain penetration (Barret et al., 2015).

2.4 Imaging modalities

2.4.1 Positron Emission Tomography (PET)

PET has been an important clinical and research tool since almost two decades. PET scanner detects the signal originating from the decay of unstable neutron deficient radioisotopes. This nuclear decay results in the emission of a positron, a particle that shares the same mass as an electron but has a positive charge on it. The emitted positron subsequently collides with a free electron resulting in annihilation creating two photons at the same time. The two photons are 180˚ apart and each carries an energy of around 511 keV which are detected by the PET scanner, a process termed coincidence logic.

A PET scanner mainly consists of a two detector system with a ring of detectors lying opposite to each other (Figure 3). This formation allows the PET scanner to form coincidences with another detector pair lying directly opposite in the ring of detectors. PET scanner also uses electronic collimation for the localization of events which is the primary reason for the high sensitivity of PET imaging.

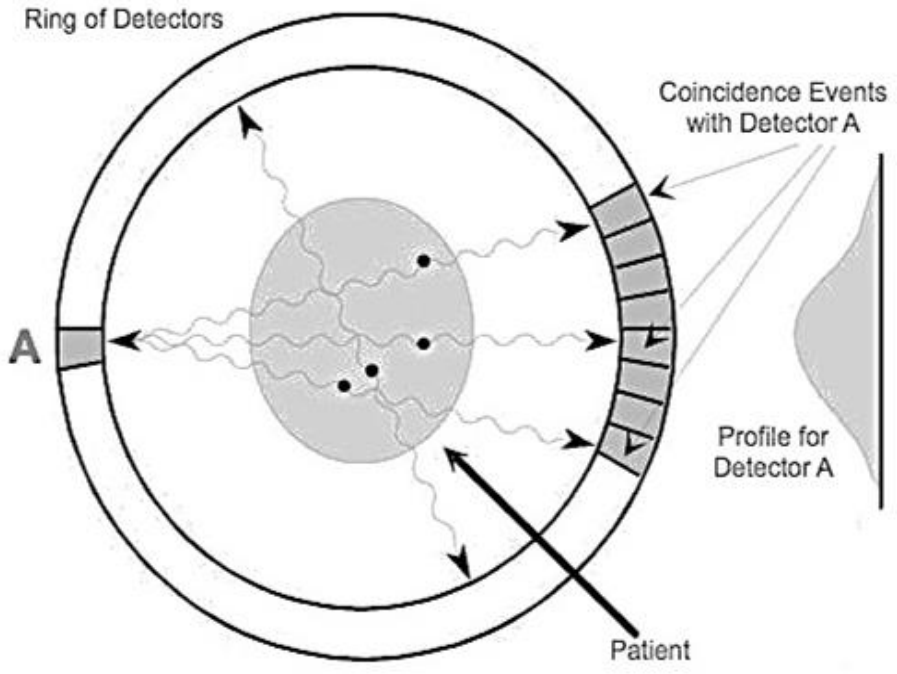

Figure 3: PET scanner ring of detectors and coincidence events
Reprinted from (Maher, 2006)

Coincidence logic or the detected photons can be mainly divided into three groups i.e. a true signal, a scatter background signal and a random background signal. In an ideal setting, two separate coincidences cannot overlap in time and the photons would not scatter within the body. Coincidences that meet these criteria are considered as a true signal. If the emitting photons undergo Compton scatter, they are known as a scattered background signal. Also, if the photons are detected close in time, they are known as a random background signal. These background signals reduce the overall quality and contrast of the PET scan. To counter these random and scattered events the detector gets rid of the signal whose energy is not equal to 511 keV and which lacks an overlapping or simultaneous time stamp. A coincidence or signal with perfect energy and time resolution is identified as a true signal.

A PET scanner is also able to locate the event relative to the mid-point between the two adjacent detectors also known as time-of-flight PET. It can be described by the following equation where the time difference (Δt) in between the detection times of two photons can be related to the origin of annihilation (Δx) relative to, as described earlier, the mid-point between two adjacent detectors. c refers to the speed of light in the equation.

$$\Delta x = (\Delta t \times c)/2$$

Image reconstruction would not be necessary because all the coincidence events could be localized in three-dimensional space, provided a perfect timing resolution is attained. Now a days, PET scanners have a timing resolution of ~375 to 600 ps. A timing resolution of ~30 ps would be needed to form the image directly without using reconstruction.

2.4.2 Magnetic Resonance Imaging (MRI)

Magnetic Resonance Imaging or MRI is an important clinical tool for non-invasive visualization of soft tissues, spinal cord and brain. It mainly involves the imaging of spinning hydrogen nucleus which is present in water, lipid and protein containing tissues. The nucleus of hydrogen atom has a small magnetic field because it is continuously spinning and has a positive charge. If placed under a magnetic field, it aligns itself in two different directions, in stark contrast to a normal compass needle. They are either arranged with or against the direction of the magnetic field (Figure 4). To put it simply, when RF

energy with Larmor frequency is applied to the protons, the ones aligned with the direction of the field, absorb this energy and switch their direction in the opposite way. After releasing this absorbed energy, the protons once again return to their original position. This 'turning back' or 'relaxation' is primarily ascertained by the T_1 and T_2 relaxation times which mainly depends on the physical and chemical composition of that particular tissue (Stanisz et al., 2005; Bottomley et al., 1987). During this relaxation phase, a tiny amount of voltage is produced by the protons in the body coil of the MRI machine. This voltage is referred to as the 'magnetic resonance signal'. In order to increase the image quality, a specialized local coil is used over the area of body to be scanned e.g. knee or spine. The main reason behind the increased contrast of MRI as compared to CT is because of the immense variation in T_1 and T_2 values. The variation in these values is much greater than those in tissue density.

An MR image is basically a visualization of signal intensities which are demonstrated by bright or dark points on the image. These points in turn depend on pulse sequence, the strength of magnetic field, blood flow, T_1, T_2 relaxation times and a couple of other factors. Images produced can either be T_1, T_2 or proton density weighted. This mainly depends on the pulse sequence as well as the repetition and echo time that is chosen.

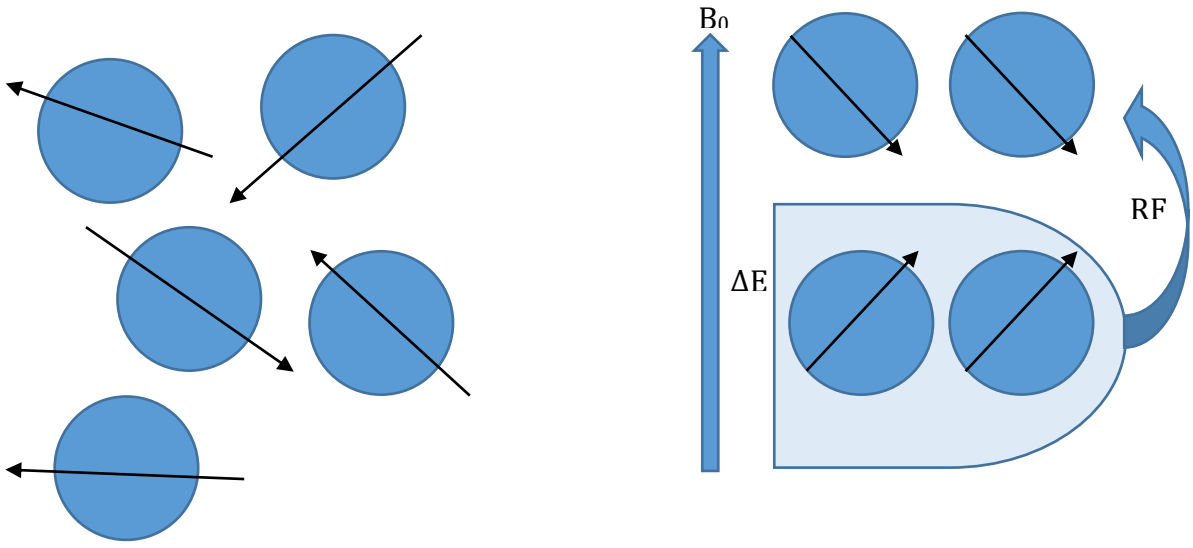

Figure 4: (LEFT) Protons randomly arranged in the absence of magnetic field. (RIGHT) In the presence of field protons are aligned towards and against the magnetic field because of the difference of energy state of these protons (E) RF frequency flips these protons into higher state of energy which also reverses their alignment. Modified from (Edelman, 1993)

Tissues with lots of free mobile water appear bright on T_2 images and dark on T_1 images. The same is true for fluids like urine and CSF although they look less dark with proton weighted images. To get an accurate diagnosis, all three types of images are taken to properly distinguish between normal and abnormal tissue e.g. in MS periventricular plaques can be distinguished from ventricular CSF with proton- density weighted images when compared with T_2 weighted images.

2.5 Compartmental/Kinetic modeling for PET tracer kinetics

As previously stated, PET allows us to trace radiotracers injected into a patient's blood with very high sensitivity. PET is being used extensively for example for detecting different cancers and following therapeutic response in cancer patients using ^{18}F-flurodeoxyglucose (^{18}F-FDG). ^{18}F-FDG has the tendency to accumulate in cancer cells because of their high metabolic demand. The resulting scan is then visually interpreted by the nuclear medicine specialist to determine whether the diagnosis is correct or if the patient is responding to the therapy. PET data, however, can be quantified for better diagnostic accuracy, for better evaluation of treatment efficacy and drug development. Although not used in routine clinical setting, compartmental model is one of the most common mathematical models that is used for quantificating PET data in research settings and for evaluating simplified quantification methods suitable for clinical use.

2.5.1 Basic concepts

A normal PET study starts after the administration of a radiopharmaceutical or radiotracer. The radiotracer itself does not indulge or interfere with normal physiological processes in the tissue under study.

Another assumption that needs to be taken into account is that the behavior of PET tracer mirrors the behavior of the receptor under study and represents its properties. Brain PET studies are an exception to this general rule.

Standardized uptake value (SUV) is the most common semi-quantitative value used for quantitating the distribution of a radioligand in a PET study (Keyes, 1995; Visser et al., 2010). It is often expressed as tissue concentration (g/ml) and can be defined with the help of a mathematical equation where TAC is the time activity curve (tissue radioactivity

concentration as a function of time; kBq/ml) measured in PET image divided by the injected dose of the radiotracer (MBq) and weight of the patient (kg).

$$SUV = \frac{TAC}{Dose/Weight}$$

As already mentioned, PET scanner detects photons emitted from the radiotracer regardless of their origin. These photons might be emitted from an unbound tracer, tracer's metabolites or from the tracer that is bound to a protein instead of its designated target.

To make sense of this abundance of signal, temporal information is needed for the tracer under study. This temporal information can only be acquired from a dynamic PET image in the form of a TAC or time-activity curve.

To acquire this TAC, input function is needed which can be taken from the arterial blood after tracer injection via repeated blood sampling at specific intervals. Input function can also be taken directly from the PET image or can be derived from previous population-based input data.

Compartmental model has some variables or parameters that directly correlate with physiological information (Watabe et al., 2006). In order to get this meaningful physiological or biochemical information one must fit the acquired TAC to a proper type of compartmental model which depends on the type of study being performed.

2.5.2 Types of compartmental models

There are three main types of compartmental models (CM) i.e. one tissue CM (Figure 5), two tissue CM and three tissue CM. Each compartment has a designated box. This box represents a pool of equally distributed tracer. Within the box, there are compartments which represent different anatomical pools within the body. The tracer moves in-between these compartments with first-order rate constant which is directly correlated to the tracer concentration within the compartment.

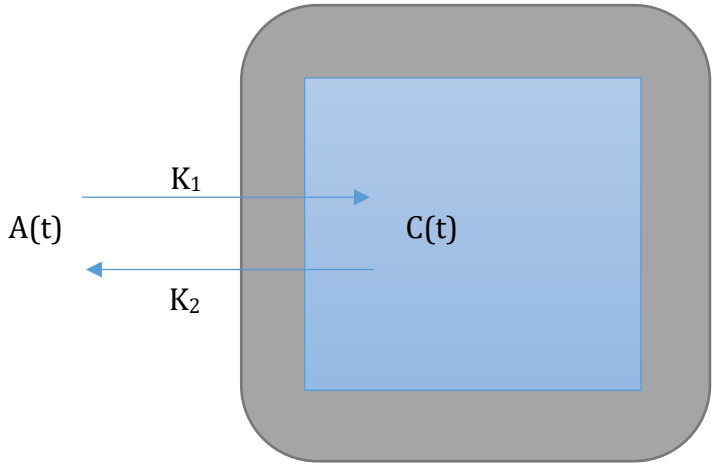

Figure 5: One-tissue compartmental model (1TCM)
Modified from (Anderson, 1983a)

One-tissue compartmental model (Figure 5) is the simplest of all compartmental models. It can be described using the following equation (2.1) where C(t) [Bq/mL] is the total time of the radiotracer in tissue as measured by positron emission tomography. A(t) represents input function with respect to time t [min]. K_1 (mL/cm^3/min] represents the rate constant i.e. blood to tissue while k_2 [l/min] represents the opposite i.e. tissue to blood. It should also be noted that K_1 is capitalized in order to differentiate it from rate constants with different units i.e. [l/min]. K_1 is a unit of volume of plasma or blood (mL) per volume of tissue (cm^3) per min.

$$\frac{dC(t)}{dt} = K_1 A(t) - k_2 C(t) \qquad (2.1)$$

One tissue compartmental model is mainly used for blood flow quantification with tracers that can diffuse freely. Commonly used tracers include [^{15}O]H_2O and [^{18}F]fluoromethane.

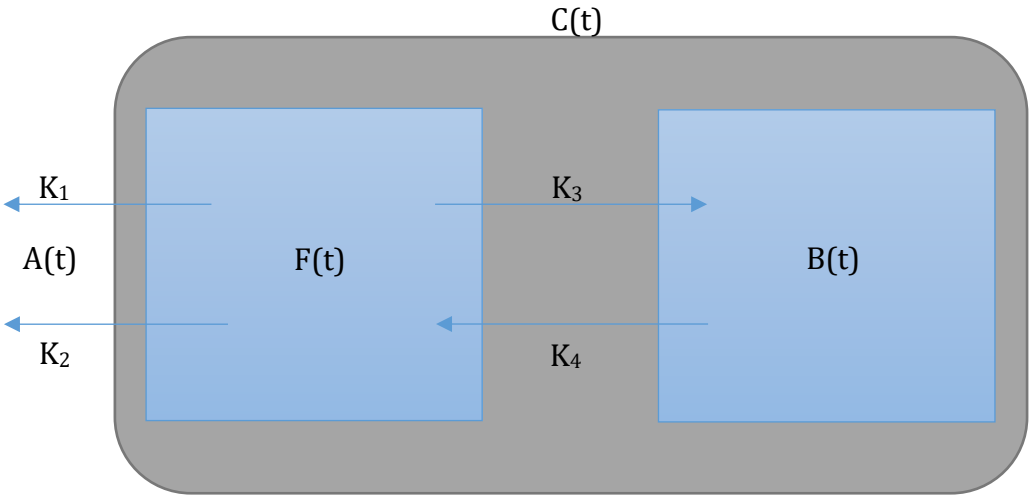

Figure 6: Two tissue comparmental model (2TCM)
Modified from (Anderson, 1983a)

Two tissue compartmental model has two compartments, as the name implies. The first one is usually referred to as the 'free compartment' while the second one as 'binding compartment'. Two differential equations (2.2 & 2.3) are needed for two compartmental model (Figure 6) for the calculation of concentration curves.

In these equations time activity curves are denoted as F(t) [Bq/ml] for the 'free compartment' and B(t) [Bq/mL] for the binding compartment. T2CM can be used for kinetic modeling of glucose phosphorylation and uptake in ^{18}F-FDG based models.

$$\frac{dF(t)}{dt} = K_1 A(t) - (k_2 + k_3)F(t) + k_4 B(t) \qquad (2.2)$$

$$\frac{dB(t)}{dt} = k_3 F(t) - k_4 B(t) \qquad (2.3)$$

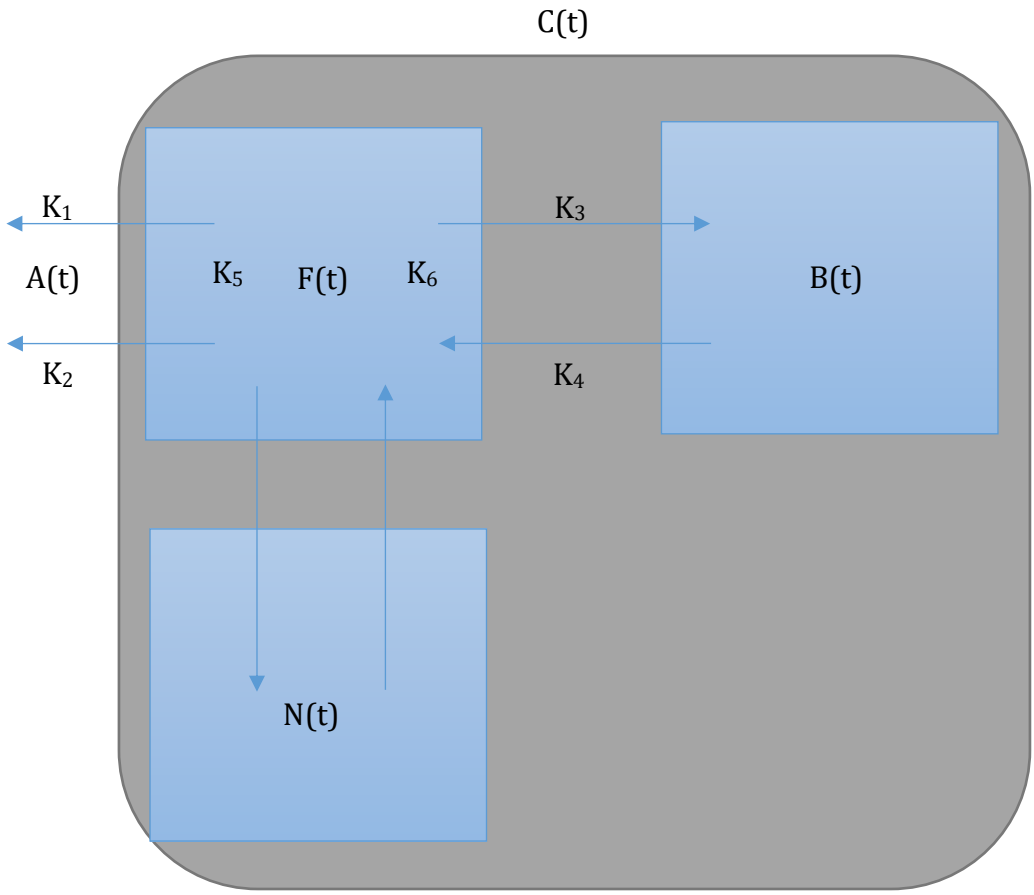

Figure 7: Three tissue compartment model (3TCM)
Modified from (Anderson, 1983b)

The 3TCM model (Figure 7), as the name implies, contains three compartments in the tissue. Time activity curves in these three compartments are F(t) [Bq/mL], B(t) [Bq/mL] and N(t) [Bq/mL] for the so-called 'free', 'specific binding' and 'non-specific binding' compartments respectively. Following equations (2.4, 2.5 & 2.6) are needed for 3TCM:

$$\frac{dF(t)}{dt} = K_1 A(t) - (k_2 + k_3 + k_5)F(t) + k_4 B(t) + k_6 N(t) \quad (2.4)$$

$$\frac{dB(t)}{dt} = k_3 F(t) - k_4 B(t) \quad (2.5)$$

$$\frac{dN(t)}{dt} = k_5 F(t) - k_6 N(t) \quad (2.5)$$

The three-tissue compartmental model is mainly used for brain receptor based studies. It is also important to note that the 3TC could also lie in series to one another. Therefore, it is necessary to specify the equations being used and the structure of the model in addition to the number of compartments.

2.5.3 Time activity curve (TAC) and Input function

Analysis of PET tracers requires the critical information of time activity curve as well as input function (Figure 8). TAC can be acquired by two main methods i.e. ROI based method and the voxel based method. In a nutshell, ROI based method involves defining a region of interest and then getting an average value of that particular region of interest (ROI). In the voxel based method, the time activity curve is taken pixel by pixel (voxel) resulting in a parametric image. Advantage of ROI based method is that it typically has less over all noise although it is more time consuming when done manually.

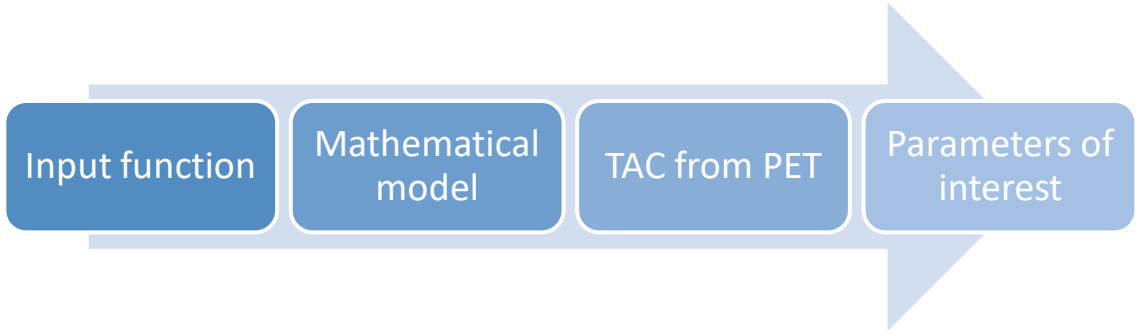

Figure 8: Schematic diagram of a typical PET study

Input function or delivery function is typically described as the total concentration of radioactivity of the intact (non-metabolized) radiotracer within the arterial plasma as a function of time. This information can be obtained by the invasive method of arterial cannulation. The method itself is not dangerous but it requires expertise. It also discourages patients and normal subjects to enroll in PET studies and exposes the researchers to unwarranted radiation. There are two non-invasive methods of acquiring input function i.e. population based input function (PBIF) and the image derived input function (IDIF). In PBIF, an average is taken of arterial input functions of previous patients and healthy volunteers and then used as input function (Eberl et al., 1997). IDIF is explained in detail in the following section.

2.6 Image derived input function

Image derived input function has been used variedly in studies that involve the use of large blood vessels such as the aorta or femoral arteries with much success. In brain studies, carotid artery is used primarily for ROI delineation. The results of brain IDIF studies have been slightly dismal because of the small caliber of carotid arteries and the presence of partial volume effects.

2.6.1 Salient features of a typical IDIF study

Multiple methods have been developed to calculate image-derived input function. In essence, there are three important steps that are common to all methods: (1) carotid ROI drawing which can be done by using co-registered MRI images or segmenting the carotids directly on the PET images. (2) Partial volume effects correction which is then used for whole blood TAC calculation. (3) Distinction of parent radiotracer from its metabolites by metabolite correction. This third step requires adequate knowledge of the dynamics of the radiotracer via blood samples as the PET scanner cannot distinguish between the original tracer, its metabolites and the resulting photons emitted (Zanotti-Fregonara et al., 2011a).

2.6.2 ICA ROI delineation

Apart from some studies that employ different methodologies to extract time activity curves e.g. Independent component analysis algorithm (Naganawa et al., 2005b), cluster analysis (Guo et al., 2007), multiple linear regression analysis (Fang et al., 2004) and dynamic factor analysis, IDIF estimation in brain PET studies usually requires manual or semiautomatic delineation of carotid artery ROI's. This step is important in attaining raw blood time activity curves. ROI's can be drawn on PET images directly or on co-registered magnetic resonance images for better recognition of carotid artery length and diameter, in theory at least.

2.6.3 Manual delineation of ROI on dynamic PET image

For using the PET data only for ROI delineation, a fast image acquisition protocol has been suggested in earlier studies. In this protocol images with frame duration as short as

2 seconds were acquired. Immediately after tracer injection, the process of acquiring images was initiated which lasted a total of 60 min duration (Chen et al., 1998). Images acquired in between 12 to 48 seconds were summed and used for ROI delineation. Each of these summed images were visually observed and ROI's were defined individually on left and/or right ICA where either or both were clearly visible. Subsequently, TAC's were generated for each separate entity. The final step is defining a certain threshold for individual pixels so that the ones having intensity above that threshold could only be used for ROI delineation. Once the ROI is delineated it is copied to the rest of the slices which may be roughly 5 to 8. A tissue ROI is further defined in close proximity to the ICA ROI for the correction of the spillover effects. In the latest, slightly modified approach to the above mentioned technique, after the visual identification of slices containing ICA, a rectangle is drawn over each of them to generate a 3D cubical space which is then used for TAC calculation (Zhou et al., 2012).

2.6.4 Automatic/semi-automatic delineation of ROI on dynamic PET image

In a study evaluating automated IDIF method for dynamic PET images in HRRT scanner, ROI's were delineated on frames that are summed early on (15 to 45 sec post injection) because ICA is visually distinguishable in them. ROI's are delineated on 11 planes starting 3 planes below the circle of willis This area corresponds to the region of ICA that is outside the skull. The selection of this area for ROI delineation helps in countering the spill in effects. There are three automatic methods which can be employed for ROI delineation all of which relate to the threshold of the individual pixels. This threshold could either be defined based on the percentage of the maximum pixel value (Method A1), number of hottest pixels in a *volume* (Method A2) or number of hottest pixels *per plane* (Method A3) (Mourik et al., 2008b).

An alternative *semi-automatic simplified seeded reference region growing* method was also investigated where only a single seed for each carotid artery was taken. The algorithm then investigates the threshold of the surrounding seeds automatically and if they pass the pre-defined threshold criteria, it adds them to the original seed till there are no more pixels to add. It should be noted however that results for both the automatic and semi-automatic methods defined in this study were not found to be consistent with the gold standard i.e. arterial input function except the automatic method A3 (four hottest pixels per plane) (Mourik et al., 2008b).

2.6.5 Delineation of ROI on dynamic PET co-registered with MRI

Methods that use PET image singularly for ROI delineation are often difficult to undertake because of low signal to noise ratio (Fung et al., 2009). In order to resolve this problem, an alternative approach of delineating ROIs on co-registered MR image was taken in some studies (Litton, 1997). In this method, ROIs were delineated as circles around the carotid arteries in the region where they don't bend both for the left and right ICA. An alternative approach is to put bounding boxes approx. 8cm (sagittal) x 4 cm (coronal) x 1.5 cm (transverse) axis. These bounding boxes were placed between the bifurcation of the external carotid and petrous segment of the internal carotid artery. Specific voxels are delineated by using different algorithms and TAC's are measured based on that delineation.

3 AIMS OF THE STUDY

The general aim of this study was to investigate whether the non-invasive method of acquiring input function i.e. image derived input function is reliable in comparison with arterial input function and population based input function for the analysis of [^{11}C]TMSX radioligand. The specific aims of this study are as follows:

I To determine which one of the two blood pools used for ROI delineation i.e. ICA or VS has better correlation with arterial input function.

II To investigate if there are any group (MS, PD, healthy controls (HC)) and sub-group (SPMS, RRMS, early stage PD (PDEA) and later stage PD without dyskinesia (PDLN)) differences in IDIF AUC's as compared with PBIF.

III To investigate if there are any age-related differences in IDIF AUC's in all pooled cases, pooled MS, pooled controls, and pooled PD cases.

4 MATERIALS AND METHODS

4.1 Study population

The [^{11}C]TMSX imaging data along with arterial input data have a been collected in previous studies conducted at Turku PET Centre (Imaging CNS adenosine receptor expression in patients with multiple sclerosis, Huntington's disease and Parkinson's disease using positron emission tomography (PET) (CADEPET)) and partly reported in earlier studies (Rissanen et al., 2013a, 2015). A combined total of 45 study subjects (Figure 10) were enrolled in the study. The MS and PD patients were enrolled from the outpatient polyclinic of the Division of Clinical Neurosciences of the Turku University Hospital. 17 patients had multiple sclerosis (MS) with 8 having relapsing remitting (RRMS) subtype of the MS and the rest with secondary progressive disease (SPMS). 19 patients with Parkinson's disease were enrolled for the study with 9 in the early stage of the disease (PDEA, disease duration of < 2 years) while the remaining 10 in the later stage of the disease but (disease duration of > 5 years) without dyskinesia (PDLN).

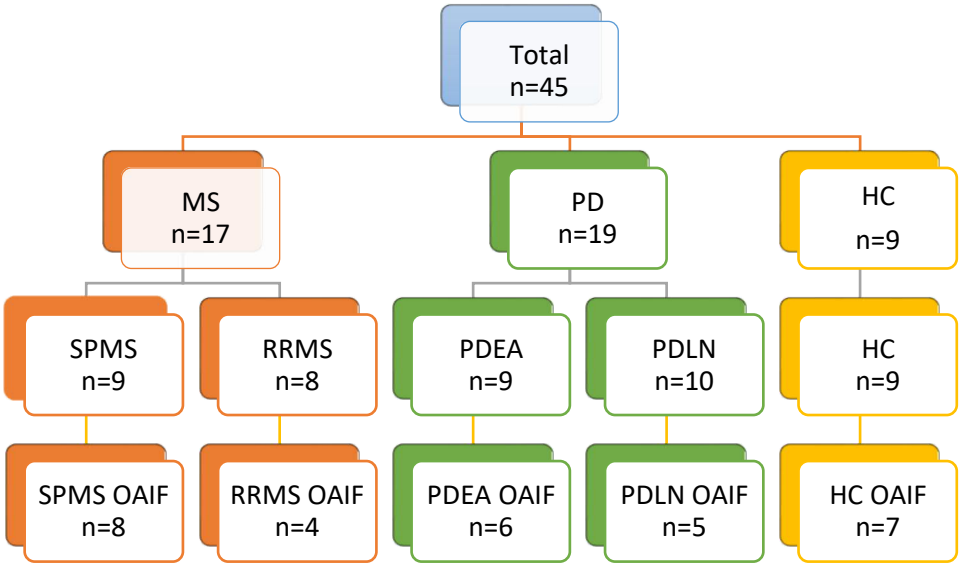

Figure 9: Study subject flow chart. SPMS= secondary progressive MS, RRMS= relapsing remitting MS, PD= Parkinson's disease, PDEA= Early stage PD, PDLN= Late stage non-dyskinetic PD, HC= healthy controls, OAIF=original artereial input function data

For comparison, imaging data was available from 9 healthy controls. Arterial input data was available for 30 of the total 45 study subjects (Figure 9). All the study participants were aged between 18 to 75 years. Pre-requisite for controls was that they had no previous history of neurological disease or symptoms. MS and PD patients were enrolled according

to the inclusion and exclusion criteria reported in earlier publications (Rissanen et al. 2013 and 2015). Medical history was taken from all study subjects on their first visit. Subjects also underwent clinical cardiovascular and neurological examination. Before entering the study, all participants provided their written, informed consent according to the principles of the Declaration of Helsinki. The CADEPET study has been approved by the Ethical Committee of the Southwestern Hospital District.

4.2 [^{11}C]TMSX Radioligand Production

[^{11}C]TMSX radioligand was synthesized locally at Turku PET Centre's radiochemistry department by using methods that have been described in detail by previous studies (Kawamura and Ishiwata, 2004).

4.3 PET and MR Image Acquisition

Dynamic PET imaging of all the study subjects were carried out at Turku PET Centre using ECAT HRRT scanner, the spatial resolution of which is approximately 2.5 mm in radial and axial directions. The field of view is usually 10 cm which covers almost all of the brain ending at the level of foramen magnum (de Jong et al., 2007). Study subjects were advised to avoid consumption of caffeine 24 hours before the scan because of the non-selective adenosine receptor antagonist properties of caffeine. An individually shaped thermoplastic face mask was used to restrict head movement during the scan. In addition, a motion detection device was used to record head movements. In the start, a transmission scan was carried out using a ^{137}Cs point source which lasted about 6 minutes and was used for attenuation correction. This was followed by a dynamic emission scan lasting 60 minutes with 27 timed frames (6 × 10, 1 × 30, 5 × 60, 5 × 150, and 8 × 300 seconds; total 3600 seconds). A bolus of [^{11}C]TMSX radiotracer was injected intravenously and initiated at simultaneously with the initiation of the dynamic imaging. An automatic arterial sampling collection system was used for taking blood samples in the initial 300 seconds of the scan which was followed by manual arterial blood sampling at 5, 10, 15, 20, 30, 40, 50 and 60 minutes. In order to calculate original arterial input function, total radioactivity concentration along with the fraction of intact radiotracer was calculated from arterial blood samples taken during the scan. In addition to that, plasma radioactivity was calculated by multiplying the total radioactivity concentration with the

mean hematocrit value (0.4). Finally, using the resulting parameters, an in house developed software was used to calculate arterial plasma input as a function of time.
MRI was performed using 1.5 T Nova Dual scanner. Axial T1 and T2, coronal FLAIR, and 3DT1 weighted in addition to DTI sequences were taken. (Rissanen et al., 2015). The 3DTI sequence was used as anatomical reference for ROI delineation.

4.4 Carotid ROI Delineation

ROI's were delineated on summed images (frames 1-12) of the dynamic PET scan with co-registered MR images (Litton, 1997; Fung et al., 2009; Mourik et al., 2009). For this purpose, an in-house developed software Carimas 2.9 was used.

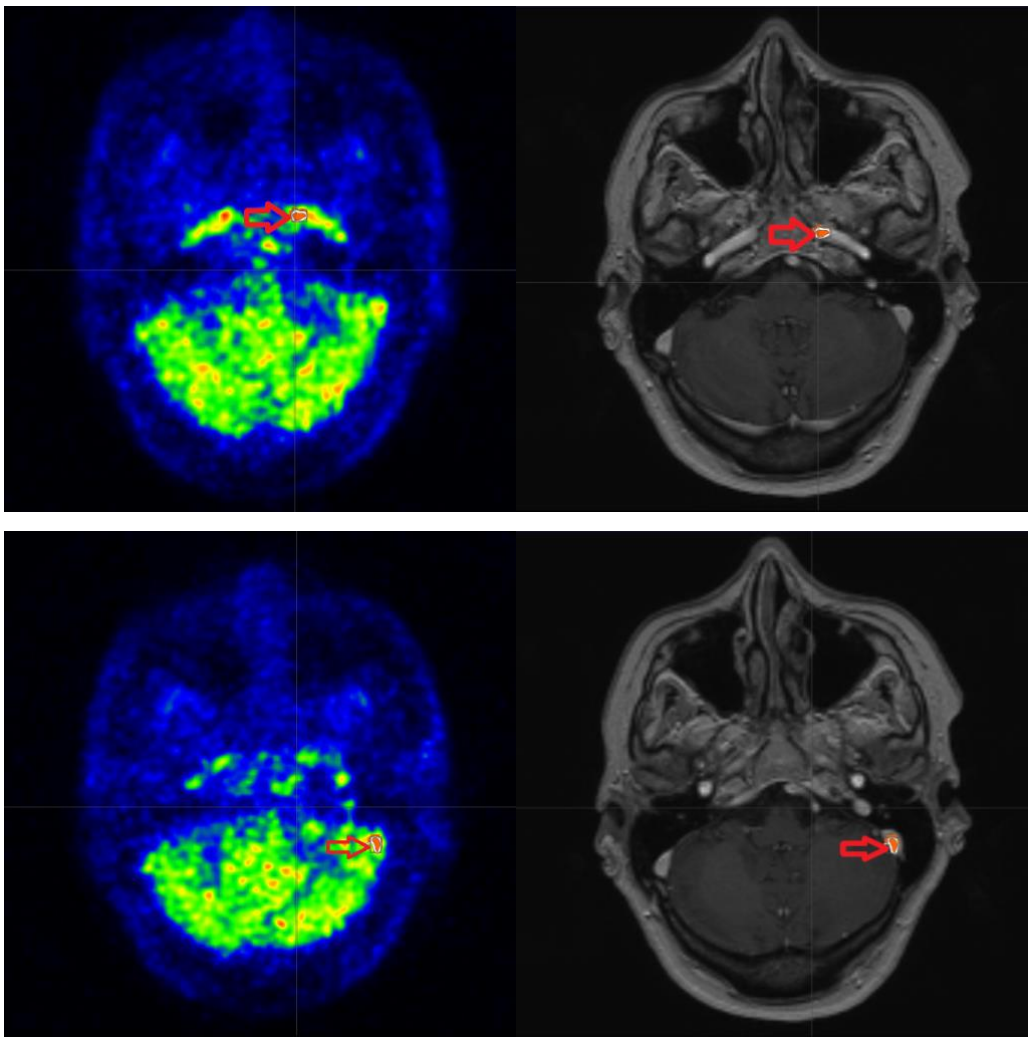

Figure 10: ROI drawn (red arrow) on PET image for ICA (top left), VS (bottom left) and checked on MRI for correct anatomical placement for ICA (top right and VS (bottom right)
ROI= region of interest, ICA= internal carotid artery, VS= transvers venous sinus, MRI= magnetic resonance imaging

Free hand tool was used to delineate ROI's on internal carotid artery just before it joins the Circle of Willis (on average at the level of trans-axial slice 31 to 32). The drawn ROI was checked with co-registered 3DTI MR image and adjusted accordingly for better anatomical accuracy (Figure 10). Similar ROI's were drawn for subsequent 5 to 8 frames depending on the signal intensity. In addition, ROI's were drawn in transverse sinuses on dynamic PET images (on average from trans-axial slice 29 onwards for subsequent 5 to 8 slices). This was also done with co-registered MRI for better anatomical detail making sure that the ROI stayed within the sinus itself. This step is necessary for the correction of 'spillover' effects of the PET signal. Finally, time activity curve (TAC) values, calculated within the Carimas software, were saved and used for data analysis.

4.5 Data Analysis

Randomized patient data including weight, height and radioligand dose administered was added in a spreadsheet in MS Excel. TAC's calculated for each subject were added separately for internal carotid artery (ICA) and transverse venous sinus (VS). The following equation (3.1) was used to calculate the standardized uptake value (SUV) in each of the 27 frames Microsoft Excel and the SUV's were then plotted on a graph with SUV on y-axis and time points on x-axis for PD and MS groups alongside controls and for both ICA and VS separately.

$$SUV = \frac{TAC}{Dose/Weight} \qquad (3.1)$$

These SUV values for both ICA and VS were metabolite corrected. This was done by writing the fraction data (derived from the arterial blood samples taken during the scan) on an ASCII file. A 'Hill type' mathematical function was applied to the fraction data. PTAC, which is also derived from the arterial blood samples, and the fitted fraction data is then used to calculate metabolite corrected plasma curve using a Turku PET Center developed script known as metabcor. The resulting values were then plotted for individual cases with original input function, PBIF, individually scaled PBIF, ICA and VS SUV values.

Furthermore, using time points (t) and TAC values, area under curve (AUC) was calculated using the trapezoidal rule (3.2) in MS Excel. These values were plotted on a line graph against time points for internal carotid artery and venous sinuses respectively.

$$AUC = \frac{(TAC_n + TAC_{n+1})}{2} \times (t_{n+1} - t_n) \qquad (3.2)$$

IDIF values were metabolite corrected and were scaled to original input function. The statistical analyses were performed using SPSS (v23). Normality of data distribution was checked using Shapiro-Wilk test. Wilcoxon signed-rank test, a non-parametric equivalent of t-test, was used to evaluate possible differences between original arterial input function, ICA_{is} and VS_{is} AUC values to determine whether the IDIF method can substitute arterial input function. Furthermore, correlations were checked between OAIF, ICA and VS AUC values using Spearman's test to determine which of the two blood pool AUC's i.e. ICA or VS correlates better with OAIF. For this comparison, the ICA and VS values were scaled to OAIF values for each individual study subject i.e. individually scaled internal carotid artery input function (ICA_{is}) and individually scaled venous sinus input function (VS_{is}).

Overall group differences between HC, MS and PD in the ICA AUC values were checked against PBIF using ANOVA with all groups pooled (HC+MS+PD). Individual paired comparison between HC, MS and PD were done to examine possible differences between groups using independent samples t-test. Subgroups (SPMS and RRMS, PDEA and PDLN) were checked for any significant differences using independent samples t-test. To calculate PBIF, Mostellar formula was used to standardize the metabolite corrected plasma time activity curve (Mosteller. R.D., 1987). The resulting curves were juxtaposed on the same time points followed by shifting them to average peak time. Lastly, they were normalized using the average of the group, excluding the single subject which was used for normalization. Individually scaled PBIF were derived from the group specific average using a non-invasive method incorporating body surface area and an invasive method using metabolite corrected arterial samples at 9 and 23 minutes which were tested to give the highest correlation with plasma AUC (Rissanen et al., 2015).

Finally, age related differences were investigated by dividing all the cases in two groups i.e. group 1 with age <45 and group 2 with age ≥45. Independent samples t-test was used

to check whether there were any significant differences between these two age groups. Spearman's correlation was also used to check any significant correlations of age to ICA AUC in individual groups i.e. HC, MS and PD.

5 RESULTS

5.1 Correlations of ICA_{is} and VS_{is} IDIF with original arterial input function

Mean and SD values of age and the SUV AUC values acquired with original arterial input data, individually scaled internal carotid artery data and individually scaled venous arterial input data is summarized in Table 4. Healthy controls mean (sd) 49 (8.3) years were age matched for SPMS patients 49 (12.2) years. RRMS patients were significantly younger, the mean age being 27.7 (7.1) years while PD patients were older than the healthy controls with the mean age of [66 (8) years. When analyzing the differences between the methods for all pooled data IDIF with ICA_{is} provided lower estimates when compared with OAIF in all groups (p= 0.004 z= -2.86). Similarly, VS_{is} also provided significantly lower estimates when compared with OAIF (p= 0.000 z= -4.86).

STUDY SUBJECTS	*All cases (n=30)*	*HC (n=7)*	*MS (pooled) (n=12)*	*SPMS (n=8)*	*RRMS (n=4)*	*PD (pooled) (n=11)*	*PDEA (n=6)*	*PDLN (n=5)*
AGE	52.4 (15.3)	49 (8.3)	42 (14.8)	49 (12.2)	27.7 (7.1)	66 (8)	63 (9.5)	69.4 (4.7)
OAIF	108.7 (17.4)	105.6 (17.6)	112.7 (18.5)	110.4 (18.3)	95.8 (12.5)	116.1 (15.1)	113.7 (17.8)	119 (12.5)
ICA_{is}	98.9 (32.1)	103.3 (45.3)	106.6 (27.5)	104.6 (26.1)	100.7 (76.8)	98.4 (20.6)	94.5 (21.1)	103.2 (21.4)
VS_{is}	64.1 (11.4)	64.1 (9.1)	61.4 (13.1)	63.8 (15.1)	56.6 (7.0)	69 (8.6)	67.4 (8.1)	70.8 (9.8)

Table 4 Mean (SD) of age and AUC values (OAIF, ICA_{is}, VS_{is}) for all study sucjects.
SPMS= secondary progressive MS, RRMS= relapsing remitting MS, PD= Parkinson's disease, PDEA= Early stage PD, PDLN= Late stage non-dyskinetic PD, HC= healthy controls, OAIF=original artereial input function data, ICA_{is}= Individually scaled internal carotid artery input data, VS_{is}= individually scaled venous sinus input data

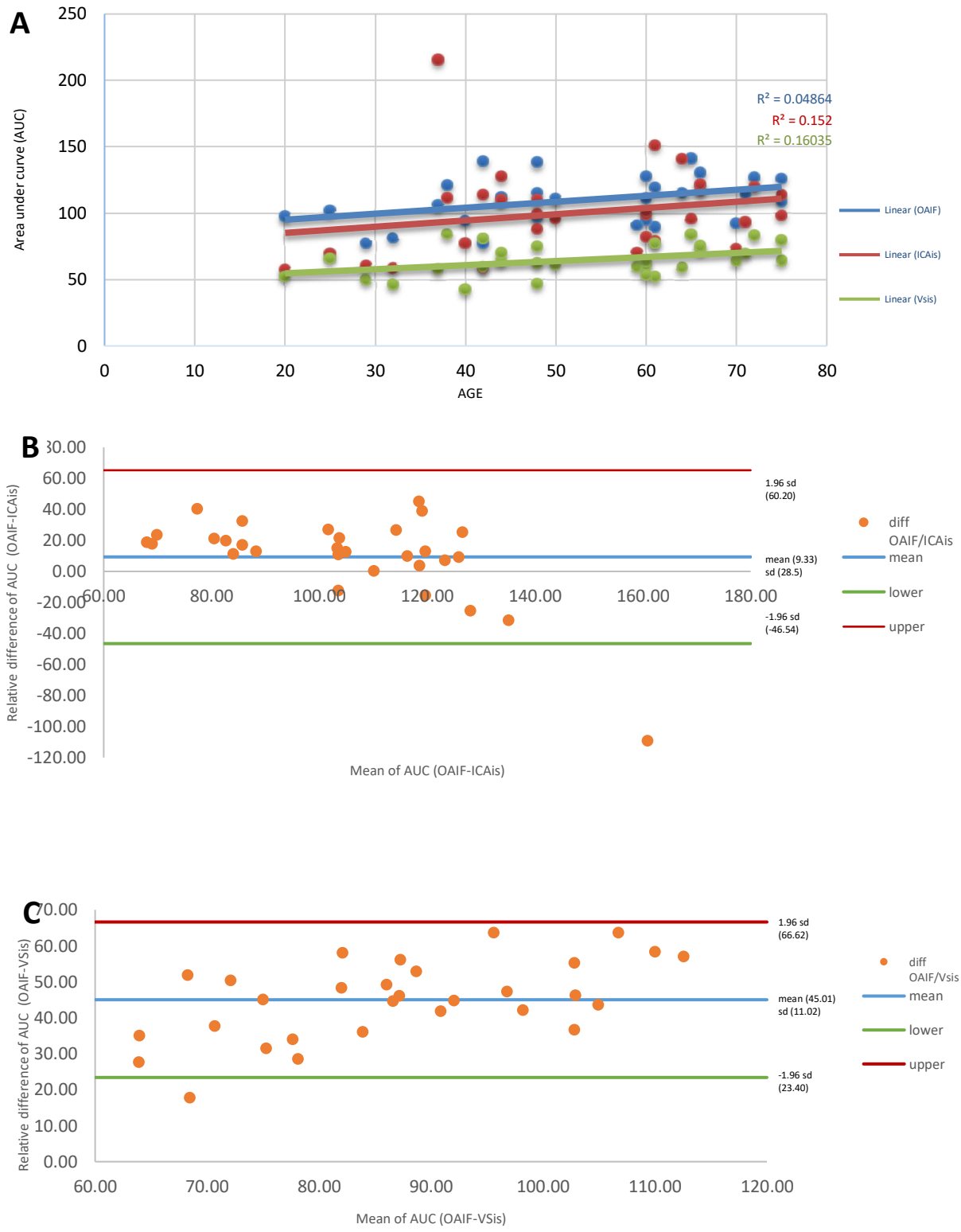

Figure 11 ***(A)*** *Correlation between age and area under curve (AUC) of original arterial input function (OAIF), individually scaled internal carotid artery (ICA_{is}) and venous sinus (VS_{is})* ***(B)*** *Bland-Altman plot showing relative difference between AUC values of ICA_{is} (relative to original input function)* ***(C)*** *Bland-Altman plot showing relative difference between AUC values of VS_{is} (relative to original input function)*

There was, however, a relatively strong correlation between individually scaled ICA AUC (ICA_{is}) and original arterial input function AUC values for all pooled subjects r (p)=

0.792 (0.000). A relatively strong correlation was also found between the individually scaled VS AUC (VS_{is}) and original arterial input function r (p)=0.686 (0.000). The correlations are visualized as Bland-Altman plots (Figure 11) demonstrating that ICA_{is} AUC correlates better with OAIF than the VS_{is}.

In group wise analysis, strong correlation was observed in healthy controls between original input data and both individually scaled ICA and VS data r (p) = **0.929 (0.003)**. Also, correlation was found to be significant in MS (pooled) r (p) = **0.657* (0.015)**, SPMS r (p) = **0.728* (0.026)**, PD (pooled) r (p) = **0.676* (0.011)**, PDEA r (p) = **0.943* (0.005)** for OI-ICA_{is} comparison and MS (pooled) r (p) = **0.847* (0.000)**, SPMS r (p) = **0.820* (0.007)**, PD (pooled) r (p) = **0.648* (0.017)** for VS_{is} comparison. Results are summarized in Table 5. In RRMS and PDLN, no significant correlations between the methods were found, which could be explained by the small number of cases in these subgroups (n=4 and n=5, respectively), and the correlation between OAIF and VSis among PDEA was not significant either (n=6).

As the ICA_{is} input data correlated better with the OAIF, the subsequent analyses in section 5.2 and 5.3 were carried out using ICA AUC values as a reference.

Group	*OAIF-ICA_{is}*	*OAIF-VS_{is}*
	Spearman (p)	***Spearman (p)***
HC	0.929* (0.003)	0.929* (0.003)
MS (pooled)	0.657* (0.015)	0.847* (0.000)
SPMS	0.728* (0.026)	0.820* (0.007)
RRMS	0.800 (0.200)	0.800 (0.200)
PD (pooled)	0.676* (0.011)	0.648* (0.017)
PDEA	0.943* (0.005)	0.600 (0.208)
PDLN	-0.300 (0.624)	0.700 (0.188)

Table 5 Correlation between Original arterial input function (OAIF) and Individually scaled Internal carotid artery input function (ICAis) in healthy controls, MS and PD groups and subgroups. Significant correlations marked with asterisk (*). SPMS= secondary progressive MS, RRMS= relapsing remitting MS, PD= Parkinson's disease, PDEA= Early stage PD, PDLN= Late stage non-dyskinetic PD, HC= healthy controls, OAIF=original arterial input data, ICA_{is}= Individually scaled internal carotid artery input data, VS_{is}= individually scaled venous sinus input data

Although we found significant differences in between overall AUC values of IDIF and original arterial input function, there were similarities found when comparing SUV curves for individual cases (Figure 12). In figure 12A the peak of individually scaled VS accurately matches the peak of original plasma input function although with a faster descending slope and a slight under estimation of the tail.

Similarly, in figure 12B individually scaled ICA and original plasma input function have a roughly similar peak with ICA having a faster descending slope and overestimation of the tail.

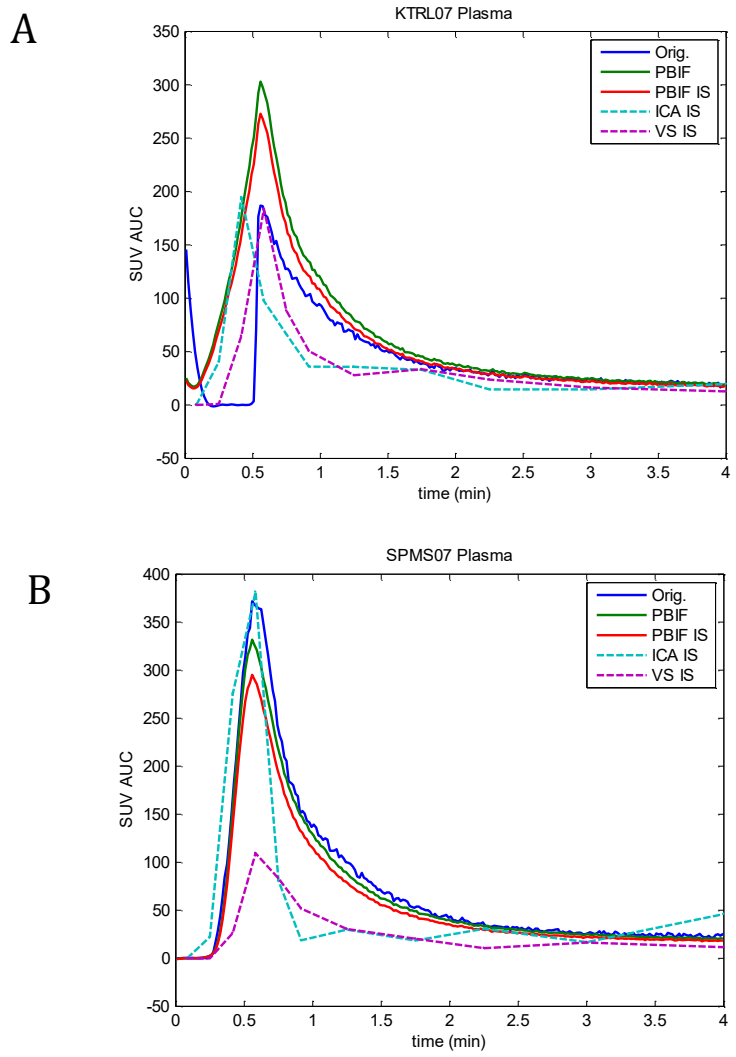

Figure 12 Standardized uptake value (SUV) comparison between original plasma input function (Orig), population based input function (PBIF), individually scaled population based input function(PBIF IS),individually scaled internal carotid artery input function (ICA IS) and individually scaled venous sinus input function (VS IS) with time in a healthy volunteer (A) and SPMS patient (B)

5.2 Group and sub-group differences in IDIF ICA AUC's and compared to PBIF

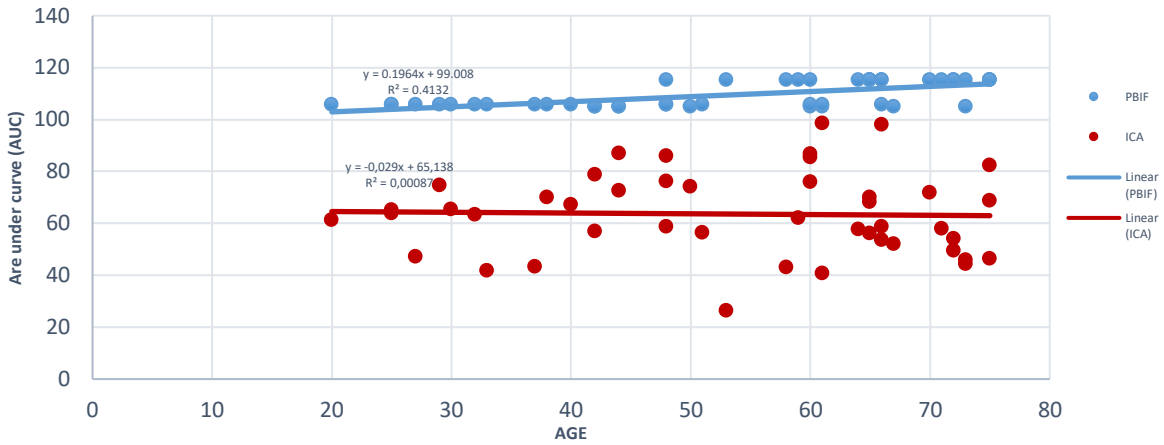

Figure 13 Scatter plot of PBIF and ICA AUC values in respect to age in all pooled cases (n=45). PBIF= population based input function, ICA= internal carotid artery, AUC=area under curve

The SUV AUC values using IDIF ICA were further evaluated for all cases (with or without arterial input) for possible mean difference within group and sub-groups against individually scaled PBIF AUC. Significant differences were found for all study subjects in between groups and within sub-groups ($p<0.05$) except for all groups pooled (HC+PD+MS) ($p=0.798$). The results are summarized in Table 6. As mentioned before, ICA input data for all study subjects was used to check group and sub group differences as it correlated better with original input data as demonstrated in section 5.1.

GROUP	*PBIF-ICA AUC Mean (SD), (p)*
All groups pooled (HC+PD+MS)	63.6 (15.9), **(0.798)**
PD (pooled)	61.7 (16.8), **(0.000)***
PDEA	70.6 (15.6), **(0.000)***
PDLN	57.2 (12.0), **(0.000)***
MS (pooled)	65.1 (15.1), **(0.000)***
SPMS	71.7(15.0), **(0.000)***
RRMS	57.8 (12.1), **(0.000)***

Table 6 Group and subgroup differences in ICA AUC values. Group differences regarded statistically significant if p<0.05 (marked with asterisk)*

5.3 Age-related association in IDIF ICA AUC's

There was no difference in the IDIF ICA AUC values with population based metabolite correction between the younger (n=15) [mean (SD) 34.07 (7.87)] and older (n=38) [63.5 (8.58)] study subjects (p=0.940).

Also, no significant age-related correlations were found in individual groups i.e. controls (r= -0.622, p= 0.074), PD (r= -0.017, p= 0.946) and MS (r= 0.422, p= 0.422). Negative trend was found between age and binding in healthy controls as demonstrated in Figure 13 (A). Scatterplots summarize the results (Figure 14).

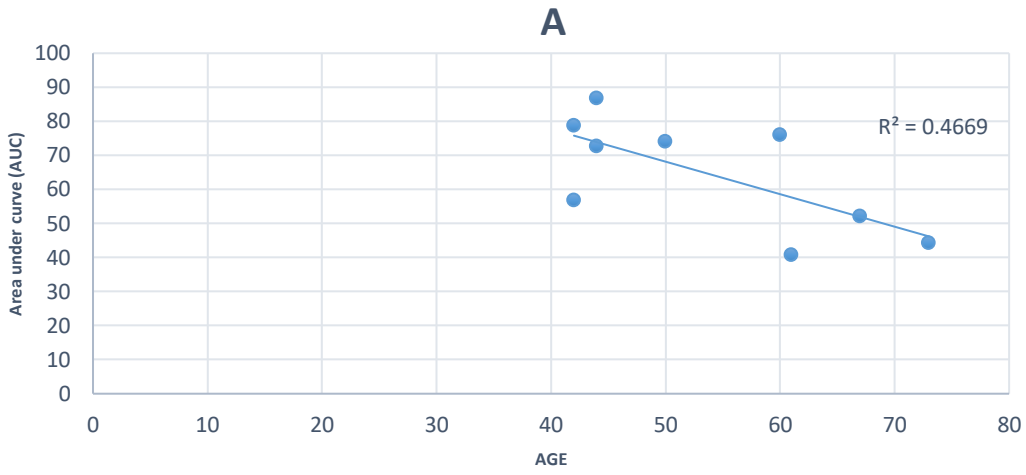

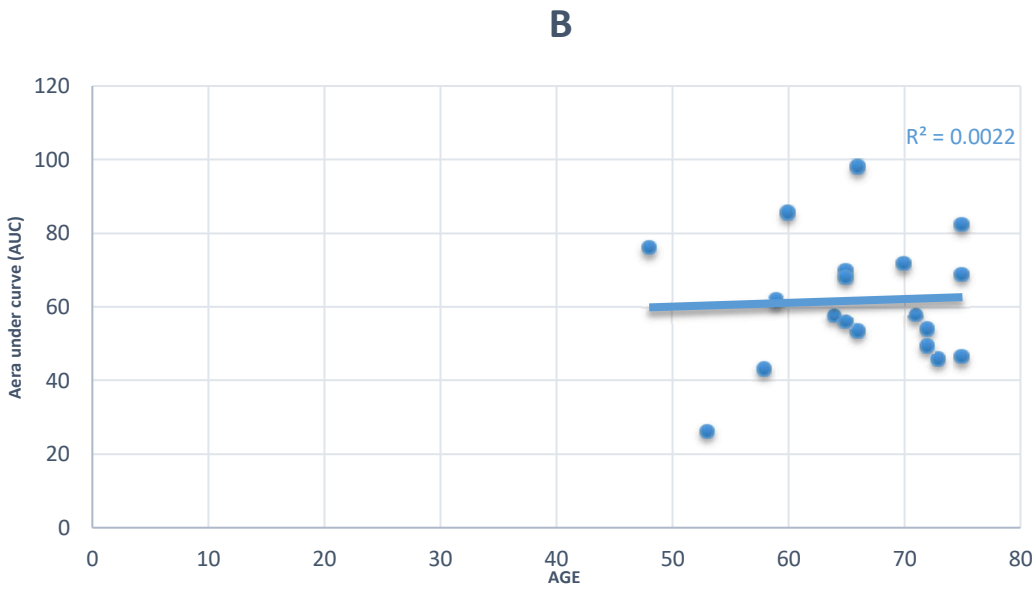

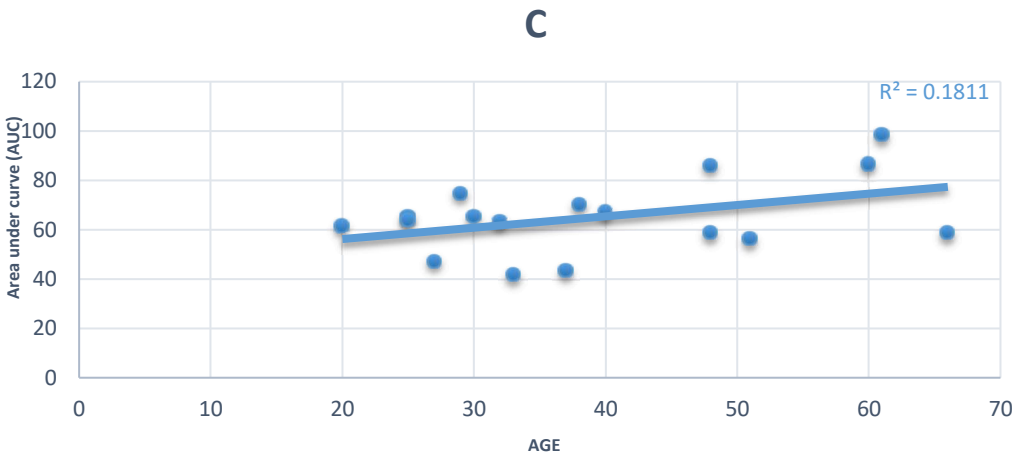

Figure 14 Age related associations in ICA AUC in (A) Healthy controls, (B) Parksinson's disease and (C) Multiple sclerosis. R^2= linear regression value

6 DISCUSSION

This study investigated an alternative approach of getting input function from the image for [^{11}C]TMSX radioligand. Various methods of acquiring input function from the image have been employed for more than a decade (Zanotti-Fregonara et al., 2009). In our study we used the method requiring the use of a co-registered MR image for better anatomical accuracy and reducing partial volume effects (Litton, 1997). Image derived input functions were converted to plasma and metabolite correction was applied to the curves (Oikonen, 2016; Kropholler et al., 2005; Hahn et al., 2012; Schain et al., 2013).

In our study we found that IDIF, although having a good correlation at group level, did not provide individually reliable estimates when compared to arterial input function and was not as accurate as the population derived input function method carried out for the same study subjects in a previous study (Rissanen et al., 2015). We used two different blood pools i.e. ICA and VS for ROI delineation which were then scaled individually with original arterial input function. We found that ICA derived input function had a much better correlation with original arterial input function after individual scaling. The inconsistency in the results could be attributed to the partial volume effect (Mourik et al., 2008a; Hahn et al., 2012; Mourik et al., 2009) (PVE) or the spill in/out effects (Lammertsma and Hume, 1996). PVE has been a major challenge in accurately quantifying the image derived input function in previous studies as well, primarily, because of the small diameter of internal carotid artery (Fung et al., 2009) and the concurrent low spatial resolution (Naganawa et al., 2005a), high signal to noise ratio (Kalk et al., 2011; Naganawa et al., 2005a; Turkheimer et al., 2007) of the PET scanner. To counter the low spatial resolution problem, HRRT scanner was used in our study. Alternatively, to avoid partial volume effects altogether, ROI's must be delineated on proximal internal carotid artery outside of the skull just after the bifurcation of common carotid artery. This is not possible with the use of HRRT scanner because it is unable to acquire images below the level of foramen magnum.

[^{11}C]TMSX tracer kinetics might also have played a part in the inaccuracy of our results primarily because of the lack of insight on how it behaves once injected into the blood stream. The usual assumption, when calculating IDIF, is that the tracer gives an accurate foreground to background ratio or in other words, has a strong carotid signal. This might not be the case with [^{11}C]TMSX because it has the tendency to bind with A_{2A} receptors

present in the blood vessel and/or it immediately diffuses into the surrounding tissues which results in weak carotid signal on which, later on, the ROI is erroneously delineated. Co-registration errors may also effect the quantification of IDIF (Fung et al., 2009; Litton, 1997) primarily because of the elastic nature of carotid artery. As the ROI on carotid artery is delineated just below the circle of Willis, the position of the artery may vary between the PET and MRI. Motion detectors were used in our study to correct positioning of internal carotid artery and to eliminate co-registration errors but ideally hybrid PET-MR machines should be used to completely eliminate this problem.

Another aspect that needed to be investigated was the age related difference in the arterial input of the [^{11}C]TMSX radiotracer. A previous study showed that there were no age related differences in the specific binding, measured as DVR for [^{11}C]TMSX radiotracer in the striatum of healthy controls (Mishina et al., 2012). Our results were in line with the former study as we did not find any age-related differences in IDIF AUC values. It goes to show that there is no difference in the arterial input of [^{11}C]TMSX radiotracer amongst different age or disease groups.

Individually scaled PBIF was considered a viable substitute for original plasma input function in a previous study (Rissanen et al., 2015). PBIF, however, is much less sensitive for individual subjects as compared to original arterial input function. We found no differences in IDIF AUC values in comparison to PBIF in our pooled study population. There were, however, differences in Parkinson's disease group which included both early onset and late onset PD patients. Also, differences were found in between early onset and late onset PD patient sub groups. Similarly, differences were found for MS patients which included both SPMS as well as RRMS patients as well as between SPMS and RRMS patient subgroups.

As shown in the comparison of SUV AUC curves for original arterial input function and individually scaled ICA and VS curves (Figure 12) the method we used can estimate IF correctly in some individual cases of healthy controls and SPMS patients. In the majority of cases during visual analysis we found that there was an overall underestimation of the peaks and over estimation of tails.

We can, therefore, conclude that the image derived input function method we evaluated, originally devised by Litton, for acquiring input function for [^{11}C]TMSX was not as

accurate as original arterial input function or population based input function validated earlier. This, however, does not mean that input function cannot be extracted from the image for [^{11}C]TMSX radiotracer as there are multiple other IF extraction methods as well. In an earlier study, input function was obtained for identical data using eight different extraction methods with only one resulting in accurate input function estimation (Zanotti-Fregonara et al., 2009). The results attained from the method devised by Litton were similar to the ones we got in our study showing underestimation of peaks and over estimation of tails of SUV curves (Figure 14). Taking this into account, the method devised by Chen (previously mentioned in section 6.3), in which only dynamic PET images were used to delineate the ROI seems like a viable alternative to the method we used in our study to derive input function. This method could be used for acquiring IDIF for [^{11}C]TMSX in future studies.

7 CONCLUSION

Although IDIF has been used extensively in previous studies for correct quantification of input function with different radioligands, in our study we have concluded that the method we used to attain it is not viable enough for [^{11}C]TMSX radioligand. Therefore, other input function extraction methods for [^{11}C]TMSX can be further investigated in future studies.

8 ACKNOWLEDGEMENTS

First and foremost, I am profoundly indebted to my supervisor Professor Laura Airas for giving me the opportunity to work alongside her and for her valuable input, support and most importantly, patience throughout the writing of this thesis.

My sincerest of gratitude to Eero Rissanen who is not just my supervisor but a mentor and a source of inspiration. This thesis would have been so much worse if it wasn't for Eero's invaluable guidance and comments. I credit him for all that is good in this thesis and take the responsibility myself for all its shortcomings.

I owe a special gratitude to my colleague Jouni Tuisku for his extensive contribution to this work. This thesis is as much his as it's mine. I would also like to thank Jouni for his encouragement and praise, especially, when it was most needed.

My sincere thanks to the faculty of BIMA especially Prof Pekka Hänninen, Prof John Eriksson and Pasi Kankaanpää. I would also like to thank Elena, Joanna and Elnaz for their immense help and support throughout the past four years.

I would also like to thank my colleagues in my group, Turku PET center and BIMA for their encouragement and support throughout the writing of this manuscript.

A special thanks to my friends at Turku PET center Kumail Motiani and Mueez Uddin for their help and advice whenever it was needed. I also have to thank my best friends Zeeshan and Umair for all the good times we had and all the great moments that await us.

Last but not the least, I would like to thank my parents Zahida and Aslam for providing me with all that life had to offer, my sister Maryam for always cheering me up and being at the other end whenever I needed to vent and Zainab for believing in me when I most doubted myself. I wouldn't be where I am if it wasn't for her. I would also like to thank my brother in law Omer for always having my back. A special thanks to Wajiha for her trust and unwavering support.

Finally, I am grateful to my niece Eeman and nephew Essa for being the joys of my life.

9 REFERENCES

Absinta, M., D.S. Reich, and M. Filippi. 2016a. Spring cleaning: time to rethink imaging research lines in MS? *J. Neurol.* 263:1893–1902. doi:10.1007/s00415-016-8060-0.

Absinta, M., P. Sati, and D.S. Reich. 2016b. Advanced MRI and staging of multiple sclerosis lesions. *Nat. Rev. Neurol.* 12:358–368. doi:10.1038/nrneurol.2016.59.

Airas, L., J. Niemelä, G. Yegutkin, and S. Jalkanen. 2007. Mechanism of action of IFN-beta in the treatment of multiple sclerosis: a special reference to CD73 and adenosine. *Ann. N. Y. Acad. Sci.* 1110:641–648. doi:10.1196/annals.1423.067.

Airas, L., E. Rissanen, and J.O. Rinne. 2015. Imaging neuroinflammation in multiple sclerosis using TSPO-PET. *Clin. Transl. Imaging*. 3:461–473. doi:10.1007/s40336-015-0147-6.

Alfaro, T.M., D.I. Rodrigues, Â.R. Tomé, R.A. Cunha, and C. Robalo Cordeiro. 2017. Adenosine A 2A receptors are up-regulated and control the activation of human alveolar macrophages. *Pulm. Pharmacol. Ther.* 45:90–94. doi:10.1016/j.pupt.2017.04.009.

Allen, I. V, S. McQuaid, M. Mirakhur, and G. Nevin. 2001. Pathological abnormalities in the normal-appearing white matter in multiple sclerosis. *Neurol. Sci.* 22:141–144. doi:10.1007/s100720170012.

Anderson, D.H. 1983a. Compartmental Modeling and Tracer Kinetics. Springer Berlin Heidelberg.

Anderson, D.H. 1983b. Compartmental Modeling and Tracer Kinetics. 50.

Augood, S.J., and P.C. Emson. 1994. Adenosine A2a receptor mRNA is expressed by enkephalin cells but not by somatostatin cells in rat striatum: a co-expression study. *Mol. Brain Res.* 22:204–210. doi:10.1016/0169-328X(94)90048-5.

Banati, R.B., J. Newcombe, R.N. Gunn, A. Cagnin, F. Turkheimer, F. Heppner, G. Price, F. Wegner, G. Giovannoni, D.H. Miller, G.D. Perkin, T. Smith, A.K. Hewson, G. Bydder, G.W. Kreutzberg, T. Jones, M.L. Cuzner, and R. Myers. 2000. The peripheral benzodiazepine binding site in the brain in multiple sclerosis Quantitative in vivo imaging of microglia as a measure of disease activity. *Brain*. 123:2321–2337. doi:10.1093/brain/123.11.2321.

Barnett, M.H., and J.W. Prineas. 2004. Relapsing and remitting multiple sclerosis. *Ann. Neurol.* 55:458–468.

Barret, O., J. Hannestad, C. Vala, D. Alagille, A. Tavares, M. Laruelle, D. Jennings, K. Marek, D. Russell, J. Seibyl, and G. Tamagnan. 2015. Characterization in humans of 18F-MNI-444, a PET radiotracer for brain adenosine 2A receptors. *J. Nucl. Med.* 56:586–91. doi:10.2967/jnumed.114.152546.

Belbasis, L., V. Bellou, E. Evangelou, J.P.A. Ioannidis, and I. Tzoulaki. 2015. Environmental risk factors and multiple sclerosis : an umbrella review of systematic reviews and meta-analyses. *Lancet Glob. Heal.* 4422:1–11. doi:10.1016/S1474-4422(14)70267-4.

Berg, D. 2006. Marker for a preclinical diagnosis of Parkinson's disease as a basis for neuroprotection. *J Neural Transm Suppl*. 123–132.

Bø, L., C. Vedeler, H. Nyland, B. Trapp, and S. Mørk. 2003. Intracortical multiple sclerosis lesions are not associated with increased lymphocyte infiltration. *Mult. Scler.* 9:323–331. doi:10.1191/1352458503ms917oa.

Bottomley, P.A., C.J. Hardy, R.E. Argersinger, and G. Allen-Moore. 1987. A Review of 1H Nuclear Magnetic Resonance Relaxation in Pathology: Are T1 and T2 Diagnostic? *Med. Phys.* 14:1–37. doi:10.1118/1.596111.

Braak, H., K. Del Tredici, U. Rüb, R.A.I. De Vos, E.N.H. Jansen Steur, and E. Braak.

2003. Staging of brain pathology related to sporadic Parkinson's disease. *Neurobiol. Aging*. 24:197–211. doi:10.1016/S0197-4580(02)00065-9.

Bynoe, M.S., C. Viret, A. Yan, and D.-G. Kim. 2015. Adenosine receptor signaling: a key to opening the blood–brain door. *Fluids Barriers CNS*. 12:20. doi:10.1186/s12987-015-0017-7.

Carman, A.J., J.H. Mills, A. Krenz, D.-G. Kim, and M.S. Bynoe. 2011. Adenosine receptor signaling modulates permeability of the blood-brain barrier. *J. Neurosci.* 31:13272–80. doi:10.1523/JNEUROSCI.3337-11.2011.

Casetta, I., F. Vincenzi, D. Bencivelli, C. Corciulo, M. Gentile, E. Granieri, P.A. Borea, and K. Varani. 2014. A2A adenosine receptors and Parkinson's disease severity. *Acta Neurol. Scand.* 129:276–281. doi:10.1111/ane.12181.

Chard, D.T., C.M. Griffin, G.J.M. Parker, R. Kapoor, a J. Thompson, and D.H. Miller. 2002. Brain atrophy in clinically early relapsing-remitting multiple sclerosis. *Brain*. 125:327–337. doi:10.1093/brain/awf025.

Chaudhuri, K.R., L. Yates, and P. Martinez-Martin. 2005. The non-motor symptom complex of Parkinson's disease: a comprehensive assessment is essential. *Curr. Neurol. Neurosci. Rep.* 5:275–283. doi:10.1007/s11910-005-0072-6.

Chen, J.F., P.K. Sonsalla, F. Pedata, A. Melani, M.R. Domenici, P. Popoli, J. Geiger, L. V. Lopes, and A. de Mendonça. 2007. Adenosine A2A receptors and brain injury: Broad spectrum of neuroprotection, multifaceted actions and "fine tuning" modulation. *Prog. Neurobiol.* 83:310–331. doi:10.1016/j.pneurobio.2007.09.002.

Chen, K., D. Bandy, E. Reiman, S.-C. Huang, M. Lawson, D. Feng, L. Yun, and A. Palant. 1998. Noninvasive quantification of the cerebral metabolic rate for glucose using positron emission tomography, 18F-fluoro-2-deoxyglucose, the Patlak method, and an image-derived input function. *J. Cereb. Blood Flow Metab.* 18:716–723. doi:10.1097/00004647-199807000-00002.

Chen, Y., R. Corriden, Y. Inoue, L. Yip, N. Hashiguchi, A. Zinkernagel, V. Nizet, P.A. Insel, and W.G. Junger. 2006. ATP release guides neutrophil chemotaxis via P2Y2 and A3 receptors. *Science*. 314:1792–5. doi:10.1126/science.1132559.

Choi, S.R., O.W. Howell, D. Carassiti, R. Magliozzi, D. Gveric, P.A. Muraro, R. Nicholas, F. Roncaroli, and R. Reynolds. 2012. Meningeal inflammation plays a role in the pathology of primary progressive multiple sclerosis. *Brain*. 135:2925–2937. doi:10.1093/brain/aws189.

Christofi, F.L., H. Zhang, J.G. Yu, J. Guzman, J. Xue, M. Kim, Y.Z. Wang, and H.J. Cooke. 2001. Differential gene expression of adenosine A1, A2a, A2b, and A3 receptors in the human enteric nervous system. *J. Comp. Neurol.* 439:46–64. doi:10.1002/cne.1334.

Coccurello, R., N. Breysse, and M. Amalric. 2004. Simultaneous blockade of adenosine A2A and metabotropic glutamate mGlu5 receptors increase their efficacy in reversing Parkinsonian deficits in rats. *Neuropsychopharmacology*. 29:1451–1461. doi:10.1038/sj.npp.1300444.

Cohen, M. V., and J.M. Downey. 2008. Adenosine: Trigger and mediator of cardioprotection. *Basic Res. Cardiol.* 103:203–215. doi:10.1007/s00395-007-0687-7.

Coles, A.J., A. Cox, E. Le Page, J. Jones, S.A. Trip, J. Deans, S. Seaman, D.H. Miller, G. Hale, H. Waldmann, and D.A. Compston. 2006. The window of therapeutic opportunity in multiple sclerosis: Evidence from monoclonal antibody therapy. *J. Neurol.* 253:98–108. doi:10.1007/s00415-005-0934-5.

Compston, A., and A. Coles. 2008. Multiple sclerosis. *Lancet*. 372:1502–17. doi:10.1016/S0140-6736(08)61620-7.

Corsi, C., a Melani, L. Bianchi, G. Pepeu, and F. Pedata. 1999. Striatal A2A adenosine receptors differentially regulate spontaneous and K+-evoked glutamate release in

vivo in young and aged rats. *Neuroreport*. 10:687–91.
Cunha, R.A., M.C. Constantino, A.M. Sebastião, and J.A. Ribeiro. 1995. Modification of A1 and A2a adenosine receptor binding in aged striatum, hippocampus and cortex of the rat. *Neuroreport*. 6:1583–8.
Dalvi, A., K.E. Lyons, and R. Pahwa. 2014. Parkinson's Disease: An Overview of Etiology, Clinical Manifestations, and Treatment. *In* Inflammation in Parkinson's Disease. Springer International Publishing, Cham. 1–24.
Dantzer, R., J.C. O'Connor, G.G. Freund, R.W. Johnson, and K.W. Kelley. 2008. From inflammation to sickness and depression: when the immune system subjugates the brain. *Nat. Rev. Neurosci.* 9:46–56. doi:10.1038/nrn2297.
Dawson, T.M., and V.L. Dawson. 2003. Rare genetic mutations shed light on the pathogenesis of Parkinson disease. *J. Clin. Invest.* 111:145–51. doi:10.1172/JCI17575.
Deckert, J., M.M. Nöthen, S.P. Bryant, S. Schuffenhauer, P.R. Schofield, N.K. Spurr, and P. Propping. 1997. Mapping of the human adenosine A 2a receptor gene: relationship to potential schizophrenia loci on chromosome 22q and exclusion from the CATCH 22 region. *Hum. Genet.* 99:326–328. doi:10.1007/s004390050366.
Deckert, J., M.M. Nothen, M. Rietschel, D. Wildenauer, B. Bondy, M.A. Ertl, M. Knapp, P.R. Schofield, M. Albus, W. Maier, and P. Propping. 1996. Human adenosine A(2a) receptor (A(2a)AR) gene: Systematic mutation screening in patients with schizophrenia. *J. Neural Transm.* 103:1447–1455. doi:10.1007/BF01271259.
Diogenes, M.J., N. ssaife-Lopes, A. Pinto-Duarte, J.A. Ribeiro, and A.M. Sebastiao. 2007. Influence of age on BDNF modulation of hippocampal synaptic transmission: interplay with adenosine A2A receptors. *Hippocampus*. 17:577–585.
Dixon, A.K., A.K. Gubitz, D.J.S. Sirinathsinghji, P.J. Richardson, and T.C. Freeman. 1996. Tissue distribution of adenosine receptor mRNAs in the rat. *Br. J. Pharmacol.* 118:1461–1468. doi:10.1111/j.1476-5381.1996.tb15561.x.
Dodd, M.L., K.J. Klos, J.H. Bower, Y.E. Geda, K.A. Josephs, and J.E. Ahlskog. 2005. Pathological gambling caused by drugs used to treat Parkinson disease. *Arch. Neurol.* 62:1377–81. doi:10.1001/archneur.62.9.noc50009.
Drayton, D.L., S. Liao, R.H. Mounzer, and N.H. Ruddle. 2006. Lymphoid organ development: from ontogeny to neogenesis. *Nat. Immunol.* 7:344–53. doi:10.1038/ni1330.
Du, C., and X. Xie. 2012. G protein-coupled receptors as therapeutic targets for multiple sclerosis. *Cell Res.* 22:1108–1128. doi:10.1038/cr.2012.87.
Duszczyszyn, D.A., J.L. Williams, H. Mason, Y. Lapierre, J. Antel, and D.G. Haegert. 2010. Thymic involution and proliferative T-cell responses in multiple sclerosis. *J. Neuroimmunol.* 221:73–80. doi:10.1016/j.jneuroim.2010.02.005.
Dutta, R., and B.D. Trapp. 2007. Pathogenesis of axonal and neuronal damage in multiple sclerosis. *In* Neurology.
Eberl, S., A.R. Anayat, R.R. Fulton, P.K. Hooper, and M.J. Fulham. 1997. Evaluation of two population-based input functions for quantitative neurological FDG PET studies. *Eur. J. Nucl. Med.* 24:299–304. doi:10.1007/s002590050056.
Edelman, R. 1993. Magnetic Resonance Imaging. *N. Engl. J. Med.* 329:434–435. doi:10.1056/NEJM199308053290616.
Fang, Y.-H., T. Kao, R.-S. Liu, and L.-C. Wu. 2004. Estimating the input function non-invasively for FDG-PET quantification with multiple linear regression analysis: simulation and verification with in vivo data. *Eur. J. Nucl. Med. Mol. Imaging*. 31:692–702. doi:10.1007/s00259-003-1412-x.
Feger, U., C. Luther, S. Poeschel, A. Melms, E. Tolosa, and H. Wiendl. 2007. Increased

frequency of CD4+ CD25+ regulatory T cells in the cerebrospinal fluid but not in the blood of multiple sclerosis patients. *Clin. Exp. Immunol.* 147:412–418. doi:10.1111/j.1365-2249.2006.03271.x.

Ferré, S., I. Diamond, S.R. Goldberg, L. Yao, S.M.O. Hourani, Z.L. Huang, Y. Urade, and I. Kitchen. 2007. Adenosine A2A receptors in ventral striatum, hypothalamus and nociceptive circuitry. Implications for drug addiction, sleep and pain. *Prog. Neurobiol.* 83:332–347. doi:10.1016/j.pneurobio.2007.04.002.

Ferreira, D.G., V.L. Batalha, H. Vicente Miranda, J.E. Coelho, R. Gomes, F.Q. Gonçalves, J.I. Real, J. Rino, A. Albino-Teixeira, R.A. Cunha, T.F. Outeiro, and L. V Lopes. 2015. Adenosine A2A Receptors Modulate α-Synuclein Aggregation and Toxicity. *Cereb. Cortex*. bhv268-. doi:10.1093/cercor/bhv268.

Franklin, R.J.M., C. ffrench-Constant, J.M. Edgar, and K.J. Smith. 2012. Neuroprotection and repair in multiple sclerosis. *Nat. Rev. Neurol.* 8:624–634. doi:10.1038/nrneurol.2012.200.

Frischer, J.M., S. Bramow, A. Dal-Bianco, C.F. Lucchinetti, H. Rauschka, M. Schmidbauer, H. Laursen, P.S. Sorensen, and H. Lassmann. 2009. The relation between inflammation and neurodegeneration in multiple sclerosis brains. *Brain*. 132:1175–1189. doi:10.1093/brain/awp070.

Fung, E.K., B. Planeta-Wilson, T. Mulnix, and R.E. Carson. 2009. A multimodal approach to image-derived input functions for brain PET. *IEEE Nucl. Sci. Symp. Conf. Rec.* 2710–2714. doi:10.1109/NSSMIC.2009.5401977.

Gasser, T. 2007. Update on the genetics of Parkinson's disease. *In* Movement Disorders.

Gauda, E.B., F.J. Northington, J. Linden, and D.L. Rosin. 2000. Differential expression of A(2a), A1-adenosine and D2-dopamine receptor genes in rat peripheral arterial chemoreceptors during postnatal development. *Brain Res.* 872:1–10. doi:10.1016/S0006-8993(00)02314-3.

Gimenez-Llort, L., S.N. Schiffmann, T. Shmidt, L. Canela, L. Camon, M. Wassholm, M. Canals, A. Terasmaa, A. Fernandez-Teruel, A. Tobena, E. Popova, S. Ferre, L. Agnati, F. Ciruela, E. Martinez, J. Scheel-Kruger, C. Lluis, R. Franco, K. Fuxe, and M. Bader. 2007. Working memory deficits in transgenic rats overexpressing human adenosine A2A receptors in the brain. *Neurobiol.Learn.Mem.* 87:42–56.

Gnad, T., S. Scheibler, I. von Kügelgen, C. Scheele, A. Kilić, A. Glöde, L.S. Hoffmann, L. Reverte-Salisa, P. Horn, S. Mutlu, A. El-Tayeb, M. Kranz, W. Deuther-Conrad, P. Brust, M.E. Lidell, M.J. Betz, S. Enerbäck, J. Schrader, G.G. Yegutkin, C.E. Müller, and A. Pfeifer. 2014. Adenosine activates brown adipose tissue and recruits beige adipocytes via A2A receptors. *Nature*. 516:395–399. doi:10.1038/nature13816.

Gosal, D., O.A. Ross, and M. Toft. 2006. Parkinson's disease: The genetics of a heterogeneous disorder. *Eur. J. Neurol.* 13:616–627. doi:10.1111/j.1468-1331.2006.01336.x.

Guo, H., R.A. Renaut, and K. Chen. 2007. An input function estimation method for FDG-PET human brain studies. *Nucl. Med. Biol.* 34:483–492. doi:10.1016/j.nucmedbio.2007.03.008.

Hahn, A., L. Nics, P. Baldinger, J. Ungersböck, P. Dolliner, R. Frey, W. Birkfellner, M. Mitterhauser, W. Wadsak, G. Karanikas, S. Kasper, and R. Lanzenberger. 2012. Combining image-derived and venous input functions enables quantification of serotonin-1A receptors with [carbonyl- 11C]WAY-100635 independent of arterial sampling. *Neuroimage*. 62. doi:10.1016/j.neuroimage.2012.04.047.

Haider, L., C. Simeonidou, G. Steinberger, S. Hametner, N. Grigoriadis, G. Deretzi, G.G. Kovacs, A. Kutzelnigg, H. Lassmann, and J.M. Frischer. 2014. Multiple sclerosis deep grey matter: the relation between demyelination, neurodegeneration,

inflammation and iron. *J. Neurol. Neurosurg. Psychiatry*. 85:1386–1395. doi:10.1136/jnnp-2014-307712.

Handel, A.E., A.J. Williamson, G. Disanto, L. Handunnetthi, G. Giovannoni, and S. V. Ramagopalan. 2010. An updated meta-analysis of risk of multiple sclerosis following infectious mononucleosis. *PLoS One*. 5:1–5. doi:10.1371/journal.pone.0012496.

Harkiolaki, M., S.L. Holmes, P. Svendsen, J.W. Gregersen, L.T. Jensen, R. McMahon, M.A. Friese, G. van Boxel, R. Etzensperger, J.S. Tzartos, K. Kranc, S. Sainsbury, K. Harlos, E.D. Mellins, J. Palace, M.M. Esiri, P.A. van der Merwe, E.Y. Jones, and L. Fugger. 2009. T Cell-Mediated Autoimmune Disease Due to Low-Affinity Crossreactivity to Common Microbial Peptides. *Immunity*. 30:348–357. doi:10.1016/j.immuni.2009.01.009.

Haskó, G., J. Linden, B. Cronstein, and P. Pacher. 2008. Adenosine receptors: therapeutic aspects for inflammatory and immune diseases. *Nat. Rev. Drug Discov.* 7:759–70. doi:10.1038/nrd2638.

Hedstrom, A.K., T. Akerstedt, J. Hillert, T. Olsson, and L. Alfredsson. 2011. Shift work at young age is associated with increased risk for multiple sclerosis. *Ann Neurol*. 70:733–741. doi:10.1002/ana.22597.

Hochmeister, S., R. Grundtner, J. Bauer, B. Engelhardt, R. Lyck, G. Gordon, T. Korosec, A. Kutzelnigg, J.J. Berger, M. Bradl, R.E. Bittner, and H. Lassmann. 2006. Dysferlin is a new marker for leaky brain blood vessels in multiple sclerosis. *J. Neuropathol. Exp. Neurol.* 65:855–865. doi:10.1097/01.jnen.0000235119.52311.16.

Howell, O.W., C.A. Reeves, R. Nicholas, D. Carassiti, B. Radotra, S.M. Gentleman, B. Serafini, F. Aloisi, F. Roncaroli, R. Magliozzi, and R. Reynolds. 2011. Meningeal inflammation is widespread and linked to cortical pathology in multiple sclerosis. *Brain*. 134:2755–2771. doi:10.1093/brain/awr182.

Howell, O.W., E.K. Schulz-Trieglaff, D. Carassiti, S.M. Gentleman, R. Nicholas, F. Roncaroli, and R. Reynolds. 2015. Extensive grey matter pathology in the cerebellum in multiple sclerosis is linked to inflammation in the subarachnoid space. *Neuropathol. Appl. Neurobiol.* 41:798–813. doi:10.1111/nan.12199.

Ingwersen, J., B. Wingerath, J. Graf, K. Lepka, M. Hofrichter, F. Schröter, F. Wedekind, A. Bauer, J. Schrader, H.-P. Hartung, T. Prozorovski, and O. Aktas. 2016. Dual roles of the adenosine A2a receptor in autoimmune neuroinflammation. *J. Neuroinflammation*. 13:48. doi:10.1186/s12974-016-0512-z.

International Multiple Sclerosis Genetics Consortium (IMSGC), Beecham AH, Patsopoulos NA, Xifara DK, Davis MF, Kemppinen A, Cotsapas C, Shah TS, Spencer C, Booth D, Goris A, Oturai A, Saarela J, Fontaine B, Hemmer B, Martin C, Zipp F, D'Alfonso S, Martine, M.J. 2013. Analysis of immune-related loci identifies 48 new susceptibility variants for multiple sclerosis. *Nat Genet*. 45:1353–1360. doi:10.1038/ng.2770.Analysis.

Ishiwata, K., M. Mishina, Y. Kimura, K. Oda, T. Sasaki, and K. Ishii. 2005. First visualization of adenosine A2A receptors in the human brain by positron emission tomography with [11C]TMSX. *Synapse*. 55:133–136. doi:10.1002/syn.20099.

Jankovic, J. 2007. Parkinson's disease: clinical features and diagnosis. doi:10.1136/jnnp.2007.131045.

Jankovic, J., and M. Stacy. 2007. Medical management of levodopa-associated motor complications in patients with Parkinson's disease. *CNS Drugs*. 21:677–692. doi:10.2165/00023210-200721080-00005.

Jenner, P., A. Mori, R. Hauser, M. Morelli, B.B. Fredholm, and J.F. Chen. 2009. Adenosine, adenosine A2A antagonists, and Parkinson's disease. *Park. Relat. Disord.* 15:406–413. doi:10.1016/j.parkreldis.2008.12.006.

de Jong, H.W.A.M., F.H.P. van Velden, R.W. Kloet, F.L. Buijs, R. Boellaard, and A.A. Lammertsma. 2007. Performance evaluation of the ECAT HRRT: an LSO-LYSO double layer high resolution, high sensitivity scanner. *Phys. Med. Biol.* 52:1505–26. doi:10.1088/0031-9155/52/5/019.

Kachroo, A., L.R. Orlando, D.K. Grandy, J.-F. Chen, A.B. Young, and M. a Schwarzschild. 2005. Interactions between metabotropic glutamate 5 and adenosine A2A receptors in normal and parkinsonian mice. *J. Neurosci.* 25:10414–10419. doi:10.1523/JNEUROSCI.3660-05.2005.

Kalk, N., E.A. Rabiner, and A.R. Lingford-Hughes. 2011. Imaging neuroinflammation in alcoholism.

Kawamura, K., and K. Ishiwata. 2004. Improved synthesis of [11C]SA4503, [11C]MPDX and [11C]TMSX by use of [11C]methyl triflate. *Ann. Nucl. Med.* 18:165–168. doi:10.1007/BF02985109.

Kenakin, T. 1995. Agonist-receptor efficacy I: mechanisms of efficacy and receptor promiscuity. *Trends Pharmacol. Sci.* 16:188–192. doi:10.1016/S0165-6147(00)89020-3.

Keyes, J.W. 1995. SUV: standard uptake or silly useless value? *J. Nucl. Med.* 36:1836–1839.

Khanapur, S., A. van Waarde, R.A.J.O. Dierckx, P.H. Elsinga, and M.J.B. Koole. 2017. Preclinical Evaluation and Quantification of ^{18}F-Fluoroethyl and ^{18}F-Fluoropropyl Analogs of SCH442416 as Radioligands for PET Imaging of the Adenosine A$_{2A}$ Receptor in Rat Brain. *J. Nucl. Med.* 58:466–472. doi:10.2967/jnumed.116.178103.

Kitada, T., S. Asakawa, N. Hattori, H. Matsumine, Y. Yamamura, S. Minoshima, M. Yokochi, Y. Mizuno, and N. Shimizu. 1998. Mutations in the parkin gene cause autosomal recessive juvenile parkinsonism. *Nature*. 392:605–608. doi:10.1038/33416.

Kondo, T., and Y. Mizuno. 2012. Safety of istradefylline (KW-6002) as adjunctive levodopa therapy in Parkinson's disease with motor complications: A combined meta-analysis of phase IIb and phase III placebocontrolled studies in Japan. *Mov. Disord.* 27:S125.

Koshiba, M., D.L. Rosin, N. Hayashi, J. Linden, and M.V.. Sitkovsky. 1999. Patterns of {A2A} Extracellular Adenosine Receptor Expression in Different Functional Subsets of Human Peripheral T Cells. Flow Cytometry Studies with {Anti-A2A} Receptor Monoclonal Antibodies. *Mol Pharmacol*. 55:614–624.

Kropholler, M.A., R. Boellaard, A. Schuitemaker, B.N.M. van Berckel, G. Luurtsema, A.D. Windhorst, and A.A. Lammertsma. 2005. Development of a tracer kinetic plasma input model for (R)-[11C]PK11195 brain studies. *J. Cereb. Blood Flow Metab.* 25:842–51. doi:10.1038/sj.jcbfm.9600092.

Kull, B.J., P.E.R. Svenningsson, and B.B. Fredholm. 2000. Adenosine A 2A Receptors are Colocalized with and Activate G olf in Rat Striatum. *Mol. Pharmacol.* 58:771–777. doi:10.1124/mol.58.4.771.

Kurihara, T., Y. Ozawa, K. Shinoda, N. Nagai, M. Inoue, Y. Oike, K. Tsubota, S. Ishida, and H. Okano. 2006. Neuroprotective effects of angiotensin II type 1 receptor (AT1R) blocker, telmisartan, via modulating AT1R and AT2R signaling in retinal inflammation. *Investig. Ophthalmol. Vis. Sci.* 47:5545–5552. doi:10.1167/iovs.06-0478.

Kutzelnigg, A., C.F. Lucchinetti, C. Stadelmann, W. Br??ck, H. Rauschka, M. Bergmann, M. Schmidbauer, J.E. Parisi, and H. Lassmann. 2005. Cortical demyelination and diffuse white matter injury in multiple sclerosis. *Brain*. 128:2705–2712. doi:10.1093/brain/awh641.

Kyowa Hakko Kirin Co., L. 2013. Kyowa Hakko Kirin - March 25, 2013 - Approval for

manufacturing and marketing of NOURIAST® tablets 20 mg, a novel antiparkinsonian agent. 1.
Lammertsma, A.A., and S.P. Hume. 1996. Simplified reference tissue model for PET receptor studies. *Neuroimage*. 4:153–8. doi:10.1006/nimg.1996.0066.
Lang, A.E., and A.M. Lozano. 1998a. Parkinson's disease. First of two parts. *N. Engl. J. Med.* 339:1044–1053. doi:10.1056/NEJM199810083391506.
Lang, A.E., and A.M. Lozano. 1998b. Parkinson's disease. Second of two parts. *N. Engl. J. Med.* 339:1130–1143. doi:10.1056/NEJM199810153391607.
Lazzarino, G., A.M. Amorini, M.J. Eikelenboom, J. Killestein, A. Belli, V. Di Pietro, B. Tavazzi, F. Barkhof, C.H. Polman, B.M.J. Uitdehaag, and A. Petzold. 2010. Cerebrospinal fluid ATP metabolites in multiple sclerosis. *Mult. Scler.* 16:549–54. doi:10.1177/1352458510364196.
Le, F., A. Townsend-Nicholson, E. Baker, G.R. Sutherland, and P.R. Schofield. 1996. Characterization and chromosomal localization of the human A2a adenosine receptor gene: ADORA2A. *Biochem Biophys Res Commun*. 223:461–467.
LeWitt, P.A., M. Guttman, J.W. Tetrud, P.J. Tuite, A. Mori, P. Chaikin, and N.M. Sussman. 2008. Adenosine A2A receptor antagonist istradefylline (KW-6002) reduces off time in Parkinson's disease: A double-blind, randomized, multicenter clinical trial (6002-US-005). *Ann. Neurol.* 63:295–302. doi:10.1002/ana.21315.
Litton, J.-E. 1997. Technical Note . Input Function in PET Brain Studies Using MR - Defined Arteries. *J. Comput. Assist. Tomogr.* 21:907–909. doi:10.1097/00004728-199711000-00012.
Lossius, A., J.N. Johansen, F. Vartdal, H. Robins, B.J. Šaltyte, T. Holmøy, and J. Olweus. 2014. High-throughput sequencing of TCR repertoires in multiple sclerosis reveals intrathecal enrichment of EBV-reactive CD8+ T cells. *Eur. J. Immunol.* 44:3439–3452. doi:10.1002/eji.201444662.
Lynge, and Hellsten. 2000. Distribution of adenosine A1, A(2A) and A(2B) receptors in human skeletal muscle. *Acta Physiol. Scand.* 169:283–290. doi:10.1046/j.1365-201X.2000.00742.x.
Maher, K. 2006. File:PetDiag2.jpg - Wikimedia Commons.
Marala, R.B., and S.J. Mustafa. 1998. Immunological characterization of adenosine A2A receptors in human and porcine cardiovascular tissues. *J. Pharmacol. Exp. Ther.* 286:1051–7.
Marrie, R.A., E. Fisher, D.M. Miller, J.C. Lee, and R.A. Rudick. 2005. Association of fatigue and brain atrophy in multiple sclerosis. *J. Neurol. Sci.* 228:161–166. doi:10.1016/j.jns.2004.11.046.
Martin, L., S.C. Pingle, D.M. Hallam, L.P. Rybak, and V. Ramkumar. 2006. Activation of the adenosine A3 receptor in RAW 264.7 cells inhibits lipopolysaccharide-stimulated tumor necrosis factor-alpha release by reducing calcium-dependent activation of nuclear factor-kappaB and extracellular signal-regulated kinase 1/2. *J. Pharmacol. Exp. Ther.* 316:71–78. doi:jpet.105.091868 [pii] 10.1124/jpet.105.091868.
McGeer, P.L., and E.G. McGeer. 2004. Inflammation and neurodegeneration in Parkinson's disease. *In* Parkinsonism and Related Disorders.
McGeer, P.L., and E.G. McGeer. 2008. Glial reactions in Parkinson's disease. *Mov. Disord.* 23:474–483. doi:10.1002/mds.21751.
Menon, S., F. Zhu, A. Shirani, J. Oger, M.S. Freedman, and H. Tremlett. 2017. Disability progression in aggressive multiple sclerosis. *Mult. Scler.* 23:456–463. doi:10.1177/1352458516653273.
Mills, J.H., L.F. Thompson, C. Mueller, A.T. Waickman, S. Jalkanen, J. Niemela, L. Airas, and M.S. Bynoe. 2008. CD73 is required for efficient entry of lymphocytes into the central nervous system during experimental autoimmune

encephalomyelitis. *Proc. Natl. Acad. Sci. U. S. A.* 105:9325–9330. doi:10.1073/pnas.0711175105.
Mishina, M., Y. Kimura, M. Naganawa, K. Ishii, K. Oda, M. Sakata, J. Toyohara, S. Kobayashi, Y. Katayama, and K. Ishiwata. 2012. Differential effects of age on human striatal adenosine A1 and A2A receptors. *Synapse*. 66:832–839. doi:10.1002/syn.21573.
Mistry, N., R. Abdel-Fahim, O. Mougin, C. Tench, P. Gowland, and N. Evangelou. 2014. Cortical lesion load correlates with diffuse injury of multiple sclerosis normal appearing white matter. *Mult. Scler. J.* 20:227–233. doi:10.1177/1352458513496344.
Mizuno, Y., and T. Kondo. 2013. Adenosine A2A receptor antagonist istradefylline reduces daily OFF time in Parkinson's disease. *Mov. Disord.* 28:1138–1141. doi:10.1002/mds.25418.
Montalban, X., M. Tintoré, J. Swanton, F. Barkhof, F. Fazekas, M. Filippi, J. Frederiksen, L. Kappos, J. Palace, C. Polman, M. Rovaris, N. De Stefano, A. Thompson, T. Yousry, A. Rovira, and D.H. Miller. 2010. MRI criteria for MS in patients with clinically isolated syndromes. *Neurology*. 74:427–434. doi:10.1212/WNL.0b013e3181cec45c.
Mori, A. 2014. Mode of action of adenosine A2A receptor antagonists as symptomatic treatment for Parkinson's disease. *Int. Rev. Neurobiol.* 119:87–116. doi:10.1016/B978-0-12-801022-8.00004-0.
Mosteller. R.D. 1987. Simplified Calculation of Body Suface Area. *N. Engl. J. Med.* 317:1098. doi:10.1056/NEJM198710223171717.
Mourik, J.E.M., M. Lubberink, U.M.H. Klumpers, E.F. Comans, A.A. Lammertsma, and R. Boellaard. 2008a. Partial volume corrected image derived input functions for dynamic PET brain studies: Methodology and validation for [11C]flumazenil. *Neuroimage*. 39:1041–1050. doi:10.1016/j.neuroimage.2007.10.022.
Mourik, J.E.M., M. Lubberink, A. Schuitemaker, N. Tolboom, B.N.M. Van Berckel, A.A. Lammertsma, and R. Boellaard. 2009. Image-derived input functions for PET brain studies. *Eur. J. Nucl. Med. Mol. Imaging*. 36. doi:10.1007/s00259-008-0986-8.
Mourik, J.E.M., F.H.P. van Velden, M. Lubberink, R.W. Kloet, B.N.M. van Berckel, A.A. Lammertsma, and R. Boellaard. 2008b. Image derived input functions for dynamic High Resolution Research Tomograph PET brain studies. *Neuroimage*. 43. doi:10.1016/j.neuroimage.2008.07.035.
MS International Federation. 2013. Atlas of MS | MS International Federation.
Multiple sclerosis in adults: management | 1-recommendations | Guidance and guidelines | NICE.
Münz, C., J.D. Lünemann, M.T. Getts, and S.D. Miller. 2009. Antiviral immune responses: triggers of or triggered by autoimmunity? *Nat. Rev. Immunol.* 9:246–58. doi:10.1038/nri2527.
Naganawa, M., Y. Kimura, Y. Manabe, and K. Chihara. 2005a. Practical Consideration about Cost Functions of Spatial Independent Component Analysis in Medical Image Processing. *Conf. Proc. IEEE Eng. Med. Biol. Soc.* 2:1120–2. doi:10.1109/IEMBS.2005.1616617.
Naganawa, M., Y. Kimura, M. Mishina, Y. Manabe, K. Chihara, K. Oda, K. Ishii, and K. Ishiwata. 2007. Quantification of adenosine A2A receptors in the human brain using [11C]TMSX and positron emission tomography. *Eur. J. Nucl. Med. Mol. Imaging*. 34:679–687. doi:10.1007/s00259-006-0294-0.
Naganawa, M., Y. Kimura, T. Nariai, K. Ishii, K. Oda, Y. Manabe, K. Chihara, and K. Ishiwata. 2005b. Omission of serial arterial blood sampling in neuroreceptor imaging with independent component analysis. *Neuroimage*. 26:885–890.

doi:10.1016/j.neuroimage.2005.02.025.
Obeso, J. a, M. Rodriguez-Oroz, C. Marin, F. Alonso, I. Zamarbide, J.L. Lanciego, and M. Rodriguez-Diaz. 2004. The origin of motor fluctuations in Parkinson's disease: importance of dopaminergic innervation and basal ganglia circuits. *Neurology*. 62:S17–S30. doi:10.1212/WNL.62.1_suppl_1.S17.
Oikonen, V. 2016. Correction of plasma TAC for metabolites.
Olson, J.K., J.L. Croxford, M.A. Calenoff, M.C. Dal Canto, and S.D. Miller. 2001. A virus-induced molecular mimicry model of multiple sclerosis. *J. Clin. Invest.* 108:311–8. doi:10.1172/JCI13032.
Palmer, T.M., and G.L. Stiles. 1997. Identification of an A(2a) adenosine receptor domain specifically responsible for mediating short-term desensitization. *Biochemistry*. 36:832–838. doi:10.1021/bi962290v.
Papadakis, M.A., S.J. McPhee, and M.W. Rabow. 2017. Current medical diagnosis & treatment 2017. 1902 pp.
Peterfreund, R.A., M. MacCollin, J. Gusella, and J.S. Fink. 1996. Characterization and expression of the human A2a adenosine receptor gene. *J. Neurochem.* 66:362–368.
Pinna, A. 2014. Adenosine A2A Receptor Antagonists in Parkinson's Disease: Progress in Clinical Trials from the Newly Approved Istradefylline to Drugs in Early Development and Those Already Discontinued. *CNS Drugs*. 28:455–474. doi:10.1007/s40263-014-0161-7.
Poewe, W. 2008. Non-motor symptoms in Parkinson's disease. *Eur. J. Neurol.* 15:14–20. doi:10.1111/j.1468-1331.2008.02056.x.
Pontieri, F.E., F. Assogna, C. Pellicano, C. Cacciari, S. Pannunzi, A. Morrone, E. Danese, C. Caltagirone, and G. Spalletta. 2015. Sociodemographic, neuropsychiatric and cognitive characteristics of pathological gambling and impulse control disorders NOS in Parkinson's disease. *Eur. Neuropsychopharmacol.* 25:69–76. doi:10.1016/j.euroneuro.2014.11.006.
Pourcher, E., H.H. Fernandez, M. Stacy, A. Mori, R. Ballerini, and P. Chaikin. 2012. Istradefylline for Parkinson's disease patients experiencing motor fluctuations: Results of the KW-6002-US-018 study. *Park. Relat. Disord.* 18:178–184. doi:10.1016/j.parkreldis.2011.09.023.
Prineas, J.W., E.E. Kwon, E.S. Cho, L.R. Sharer, M.H. Barnett, E.L. Oleszak, B. Hoffman, and B.P. Morgan. 2001. Immunopathology of secondary-progressive multiple sclerosis. *Ann. Neurol.* 50:646–657. doi:10.1002/ana.1255.
Ramlackhansingh, A.F., S.K. Bose, I. Ahmed, F.E. Turkheimer, N. Pavese, and D.J. Brooks. 2011. Adenosine 2A receptor availability in dyskinetic and nondyskinetic patients with Parkinson disease. *Neurology*. 76:1811–1816. doi:10.1212/WNL.0b013e31821ccce4.
Ransohoff, R.M. 2016. How neuroinflammation contributes to neurodegeneration. *Science (80-.).* 353:777–783. doi:10.1126/science.aag2590.
Richardson, P.J., A.K. Dixon, K. Lee, M.I. Bell, P.J. Cox, R. Williams, R.D. Pinnock, and T.C. Freeman. 2000. Correlating physiology with gene expression in striatal cholinergic neurones. *J. Neurochem.* 74:839–846. doi:10.1046/j.1471-4159.2000.740839.x.
Ridder, D.A., and M. Schwaninger. 2012. In search of the neuroprotective mechanism of thiazolidinediones in Parkinson's disease. *Exp. Neurol.* 238:133–137. doi:10.1016/j.expneurol.2012.08.012.
Rissanen, E., J. Tuisku, P. Luoto, E. Arponen, J. Johansson, V. Oikonen, R. Parkkola, L. Airas, and J.O. Rinne. 2015. Automated Reference Region Extraction and Population-Based Input Function for Brain [^{11} C]TMSX PET Image Analyses. *J. Cereb. Blood Flow Metab.* 35:157–165. doi:10.1038/jcbfm.2014.194.
Rissanen, E., J.R. Virta, T. Paavilainen, J. Tuisku, S. Helin, P. Luoto, R. Parkkola, J.O.

Rinne, and L. Airas. 2013a. Adenosine A2A Receptors in Secondary Progressive Multiple Sclerosis: A [11C]TMSX Brain PET Study. *J. Cereb. Blood Flow Metab.* 33:1394–1401. doi:10.1038/jcbfm.2013.85.

Rissanen, E., J.R. Virta, T. Paavilainen, J. Tuisku, S. Helin, P. Luoto, R. Parkkola, J.O. Rinne, and L. Airas. 2013b. Adenosine A2A Receptors in Secondary Progressive Multiple Sclerosis: A [11C]TMSX Brain PET Study. *J. Cereb. Blood Flow Metab.* 33:1394–1401. doi:10.1038/jcbfm.2013.85.

Rosin, D.L., A. Robeva, R.L. Woodard, P.G. Guyenet, and J. Linden. 1998. Immunohistochemical localization of adenosine A2A receptors in the rat central nervous system. *J Comp Neurol*. 401:163–186. doi:10.1002/(SICI)1096-9861(19981116)401:2<163::AID-CNE2>3.0.CO;2-D [pii].

Ryzhov, S., S. V Novitskiy, R. Zaynagetdinov, A.E. Goldstein, D.P. Carbone, I. Biaggioni, M.M. Dikov, and I. Feoktistov. 2008. Host A(2B) adenosine receptors promote carcinoma growth. *Neoplasia*. 10:987–995. doi:10.1593/neo.08478.

Saavedra, J.M. 2012. Angiotensin II AT(1) receptor blockers as treatments for inflammatory brain disorders. *Clin. Sci. (Lond).* 123:567–90. doi:10.1042/CS20120078.

Sakata, M., K. Ishibashi, M. Imai, K. Wagatsuma, K. Ishii, X. Zhou, E.F. de Vries, P.H. Elsinga, K. Ishiwata, and J. Toyohara. 2017a. Initial Evaluation of a Novel Adenosine A $_{2A}$ Receptor Ligand, ^{11} C-Preladenant, in Healthy Human Subjects. *J. Nucl. Med.* jnumed.116.188474. doi:10.2967/jnumed.116.188474.

Sakata, M., K. Ishibashi, M. Imai, K. Wagatsuma, K. Ishii, X. Zhou, E.F.J. De Vries, P.H. Elsinga, K. Ishiwata, and J. Toyohara. 2017b. Initial evaluation of an adenosine A<inf>2A</inf> receptor ligand, ^{11}C-preladenant, in healthy human subjects. *J. Nucl. Med.* 58. doi:10.2967/jnumed.116.188474.

Schain, M., S. Benjaminsson, K. Varnäs, A. Forsberg, C. Halldin, A. Lansner, L. Farde, and A. Varrone. 2013. Arterial input function derived from pairwise correlations between PET-image voxels. *J. Cereb. Blood Flow Metab.* 33. doi:10.1038/jcbfm.2013.47.

Schwab, C., and P.L. McGeer. 2008. Inflammatory aspects of Alzheimer disease and other neurodegenerative disorders. *J. Alzheimers. Dis.* 13:359–369.

Sexl, V., G. Mancusi, C. Höller, E. Gloria-Maercker, W. Schütz, and M. Freissmuth. 1997. Stimulation of the mitogen-activated protein kinase via the A2A-adenosine receptor in primary human endothelial cells. *J. Biol. Chem.* 272:5792–9. doi:10.1074/jbc.272.9.5792.

Shulman, J.M., P.L. De Jager, and M.B. Feany. 2011. Parkinson's disease: genetics and pathogenesis. *Annu. Rev. Pathol.* 6:193–222. doi:10.1146/annurev-pathol-011110-130242.

Shults, C.W. 2006. Lewy bodies. *Proc. Natl. Acad. Sci. U. S. A.* 103:1661–8. doi:10.1073/pnas.0509567103.

Siderowf, A., and M.B. Stern. 2006. Preclinical diagnosis of Parkinson's disease: Are we there yet? *Curr. Neurol. Neurosci. Rep.* 6:295–301. doi:10.1007/s11910-006-0021-z.

Spratt, D.E., M.-T. RJ, Y.J. Noh, P. Mercier, N. Manczyk, K.R. Barber, J.D. Aguirre, L. Burchell, A. Purkiss, H. Walden, and G.S. Shaw. 2013. A molecular explanation for the recessive nature of parkin-linked Parkinson's disease. *Nat Commun*. 4:1983. doi:10.1038/ncomms2983.

Stamey, W., and J. Jankovic. 2008. Impulse control disorders and pathological gambling in patients with Parkinson disease. *Neurologist*. 14:89–99. doi:10.1097/NRL.0b013e31816606a7.

Stanisz, G.J., E.E. Odrobina, J. Pun, M. Escaravage, S.J. Graham, M.J. Bronskill, and R.M. Henkelman. 2005. T1, T2 relaxation and magnetization transfer in tissue at

3T. *Magn. Reson. Med.* 54:507–512. doi:10.1002/mrm.20605.
Steeves, T.D.L., J. Miyasaki, M. Zurowski, A.E. Lang, G. Pellecchia, T. Van Eimeren, P. Rusjan, S. Houle, and A.P. Strafella. 2009. Increased striatal dopamine release in Parkinsonian patients with pathological gambling: A [11C] raclopride PET study. *Brain*. 132:1376–1385. doi:10.1093/brain/awp054.
Stehle, J.H., S.A. Rivkees, J.J. Lee, D.R. Weaver, J.D. Deeds, and S.M. Reppert. 1992. Molecular cloning and expression of the cDNA for a novel A2-adenosine receptor subtype. *Mol Endocrinol*. 6:384–393.
Sullivan, G.W., J.M. Rieger, W. Michael Scheld, T.L. Macdonald, and J. Linden. 2001. Cyclic AMP-dependent inhibition of human neutrophil oxidative activity by substituted 2-propynylcyclohexyl adenosine A 2A receptor agonists. *Br. J. Pharmacol.* 132:1017–1026. doi:10.1038/sj.bjp.0703893.
Takahashi, R.N., F.A. Pamplona, and R.D.S. Prediger. 2008. Adenosine receptor antagonists for cognitive dysfunction: a review of animal studies. *Front. Biosci.* 13:2614–32. doi:10.2741/2870.
Taomoto, M., D.S. McLeod, C. Merges, and G.A. Lutty. 2000. Localization of adenosine A2a receptor in retinal development and oxygen-induced retinopathy. *Investig. Ophthalmol. Vis. Sci.* 41:230–243.
Thompson, A.J., B.L. Banwell, F. Barkhof, W.M. Carroll, T. Coetzee, G. Comi, J. Correale, F. Fazekas, M. Filippi, M.S. Freedman, K. Fujihara, S.L. Galetta, H.P. Hartung, L. Kappos, F.D. Lublin, R.A. Marrie, A.E. Miller, D.H. Miller, X. Montalban, E.M. Mowry, P.S. Sorensen, M. Tintoré, A.L. Traboulsee, M. Trojano, B.M.J. Uitdehaag, S. Vukusic, E. Waubant, B.G. Weinshenker, S.C. Reingold, and J.A. Cohen. 2018. Diagnosis of multiple sclerosis: 2017 revisions of the McDonald criteria. *Lancet Neurol.* 17:162–173. doi:10.1016/S1474-4422(17)30470-2.
Toufektsian, M.-C. 2005. Stimulation of A2A-adenosine receptors after myocardial infarction suppresses inflammatory activation and attenuates contractile dysfunction in the remote left ventricle. *AJP Hear. Circ. Physiol.* 290:H1410–H1418. doi:10.1152/ajpheart.00860.2005.
Tumani, H., H.-P. Hartung, B. Hemmer, C. Teunissen, F. Deisenhammer, G. Giovannoni, and U.K. Zettl. 2009. Cerebrospinal fluid biomarkers in multiple sclerosis. *Neurobiol. Dis.* 35:117–27. doi:10.1016/j.nbd.2009.04.010.
Turkheimer, F.E., P. Edison, N. Pavese, F. Roncaroli, A.N. Anderson, A. Hammers, A. Gerhard, R. Hinz, Y.F. Tai, and D.J. Brooks. 2007. Reference and target region modeling of [11C]-(R)-PK11195 brain studies. *J. Nucl. Med.* 48:158–167. doi:48/1/158 [pii].
Ulusoy, G.K., T. Celik, H. Kayir, M. Gürsoy, A.T. Isik, and T.I. Uzbay. 2011. Effects of pioglitazone and retinoic acid in a rotenone model of Parkinson's disease. *Brain Res. Bull.* 85:380–384. doi:10.1016/j.brainresbull.2011.05.001.
Viglietta, V., C. Baecher-Allan, H.L. Weiner, and D.A. Hafler. 2004. Loss of functional suppression by CD4+CD25+ regulatory T cells in patients with multiple sclerosis. *J. Exp. Med.* 199:971–9. doi:10.1084/jem.20031579.
Vincenzi, F., C. Corciulo, M. Targa, S. Merighi, S. Gessi, I. Casetta, M. Gentile, E. Granieri, P.A. Borea, and K. Varani. 2013. Multiple sclerosis lymphocytes upregulate A2A adenosine receptors that are antiinflammatory when stimulated. *Eur. J. Immunol.* 43:2206–2216. doi:10.1002/eji.201343314.
Visser, E.P., O.C. Boerman, and W.J.G. Oyen. 2010. SUV: From Silly Useless Value to Smart Uptake Value. *J. Nucl. Med.* 51:173–175. doi:10.2967/jnumed.109.068411.
Voon, V., and S.H. Fox. 2007. Medication-related impulse control and repetitive behaviors in Parkinson disease. *Arch. Neurol.* 64:1089–1096. doi:10.1097/WCO.0b013e32826fbc8f.
Wakabayashi, K., K. Tanji, F. Mori, and H. Takahashi. 2007. The Lewy body in

Parkinson's disease: Molecules implicated in the formation and degradation of ??-synuclein aggregates. *In* Neuropathology. 494–506.
Waldner, H., M. Collins, and V.K. Kuchroo. 2004. Activation of antigen-presenting cells by microbial products breaks self tolerance and induces autoimmune disease. *J. Clin. Invest.* 113:990–997. doi:10.1172/JCI200419388.
Watabe, H., Y. Ikoma, Y. Kimura, M. Naganawa, and M. Shidahara. 2006. PET kinetic analysis - Compartmental model. *Ann. Nucl. Med.* 20:583–588. doi:10.1007/BF02984655.
Weintraub, D., C.L. Comella, and S. Horn. 2008. Parkinson's disease--Part 3: Neuropsychiatric symptoms. *Am. J. Manag. Care*. 14:S59-69. doi:10177 [pii].
Weintraub, D., J. Koester, M.N. Potenza, A.D. Siderowf, M. Stacy, V. Voon, J. Whetteckey, G.R. Wunderlich, and A.E. Lang. 2010. Impulse control disorders in Parkinson disease: a cross-sectional study of 3090 patients. *Arch. Neurol.* 67:589–95. doi:10.1001/archneurol.2010.65.
Woulfe, J.M., M.T. Gray, D.A. Gray, D.G. Munoz, and J.M. Middeldorp. 2014. Hypothesis: A role for EBV-induced molecular mimicry in Parkinson's disease. *Park. Relat. Disord.* 20:685–694. doi:10.1016/j.parkreldis.2014.02.031.
Xiromerisiou, G., E. Dardiotis, V. Tsimourtou, P.M. Kountra, K.N. Paterakis, E.Z. Kapsalaki, K.N. Fountas, and G.M. Hadjigeorgiou. 2010. Genetic basis of Parkinson disease. *Neurosurg. Focus*. 28:E7. doi:10.3171/2009.10.FOCUS09220.
Yao, S.-Q., Z.-Z. Li, Q.-Y. Huang, F. Li, Z.-W. Wang, E. Augusto, J.-C. He, X.-T. Wang, J.-F. Chen, and R.-Y. Zheng. 2012. Genetic inactivation of the adenosine A(2A) receptor exacerbates brain damage in mice with experimental autoimmune encephalomyelitis. *J. Neurochem.* 123:100–12. doi:10.1111/j.1471-4159.2012.07807.x.
Ylikotila, P., T. Tiirikka, J.S. Moilanen, H. Kääriäinen, R. Marttila, and K. Majamaa. 2015. Epidemiology of early-onset Parkinson's disease in Finland. *Park. Relat. Disord.* 21:938–942. doi:10.1016/j.parkreldis.2015.06.003.
Zanotti-Fregonara, P., K. Chen, J.S. Liow, M. Fujita, and R.B. Innis. 2011a. Image-derived input function for brain PET studies: many challenges and few opportunities. *J Cereb Blood Flow Metab*. 31:1986–1998. doi:10.1038/jcbfm.2011.107.
Zanotti-Fregonara, P., E.M. Fadaili, R. Maroy, C. Comtat, A. Souloumiac, S. Jan, M.-J. Ribeiro, V. Gaura, A. Bar-Hen, and R. Trébossen. 2009. Comparison of Eight Methods for the Estimation of the Image-Derived Input Function in Dynamic [^{18} F]-FDG PET Human Brain Studies. *J. Cereb. Blood Flow Metab.* 29:1825–1835. doi:10.1038/jcbfm.2009.93.
Zanotti-Fregonara, P., S.S. Zoghbi, J.S. Liow, E. Luong, R. Boellaard, R.L. Gladding, V.W. Pike, R.B. Innis, and M. Fujita. 2011b. Kinetic analysis in human brain of [11C](R)-rolipram, a positron emission tomographic radioligand to image phosphodiesterase 4: A retest study and use of an image-derived input function. *Neuroimage*. 54. doi:10.1016/j.neuroimage.2010.10.064.
Zhou, S., K. Chen, E.M. Reiman, D. Li, and B. Shan. 2012. A method for generating image-derived input function in quantitative 18F-FDG PET study based on the monotonicity of the input and output function curve. *Nucl. Med. Commun.* 33:362–70. doi:10.1097/MNM.0b013e32834f262e.
Zhou, X., S. Khanapur, J.R. de Jong, A.T. Willemsen, R.A. Dierckx, P.H. Elsinga, and E.F. de Vries. 2017. In vivo evaluation of [^{11} C]preladenant positron emission tomography for quantification of adenosine A $_{2A}$ receptors in the rat brain. *J. Cereb. Blood Flow Metab.* 37:577–589. doi:10.1177/0271678X16634714.